A Project Report on

Development of an Application Oriented Solar Powered UAV

By

Mr. Anuj Naik (B150450918)
Mr. Malhar Pagedar (B150450924)
Mr. Jayant Palde (B150450926)
Mr. Raunak Supekar (B150450967)

Guide

Dr. P. S. Purandare

Department of Mechanical Engineering

Marathwada Mitra Mandal's

College of Engineering, Pune

[2018-19]

Marathwada Mitra Mandal's

College of Engineering, Pune

Karvenagar, Pune

C E R T I F I C A T E

This is to certify that the group of **Mr. Anuj Naik (B150450918), Mr. Malhar Pagedar (B150450924), Mr. Jayant Palde (B150450926) and Mr. Raunak Supekar (B150450967),** have successfully completed the Project entitled **"Development of an Application Oriented Solar Powered UAV"**, under my supervision, in the partial fulfillment of Bachelor of Engineering - Mechanical Engineering of **Savitribai Phule Pune University**.
Date: 07/06/2019

Place: PUNE

Dr. P.S. Purandare	Dr. S. M. Deshpande
Guide & Head of Department,	
Mechanical Engg.	Principal
MMCOE, Pune	MMCOE, Pune

ACKNOWLEGDEMENT

We are highly indebted to **Dr. P.S. Purandare** for his guidance and supervision, as well as for providing us with necessary information and his support in completing the project.

We would like to express our gratitude towards our parents & staff members of Mechanical Branch for their kind co-operation and encouragement which helped us in completion of this project.

Our thanks and appreciations also go to people who have willingly helped us out with their abilities. It would not have been possible without the kind support and help of many individuals and organizations.

We would like to extend our sincere thanks to all of them.

Yours Sincerely,

Mr. Anuj Naik (B150450918)
Mr. Malhar Pagedar (B150450924)
Mr. Jayant Palde (B150450926)
Mr. Raunak Supekar (B150450967)

INDEX

LIST OF FIGURES

LIST OF TABLES

ABSTRACT

The main objective of this project is to create a platform for an application based Solar Powered Unmanned Ariel Vehicle (UAV). This model acts as a sustainable benchmark for various industries, which can be further modified and also scaled up as per the applications and requirements.

This is a solar-electric model, which uses a glider configuration with fixed wings, has photovoltaic cells on them which gather solar energy thereby recharging the batteries that powers its propellers via an electric motor. This will enable the model for prolonged flights due to increased area and gliding tendency, thus minimising the overall energy costs (including fuel and battery charging cost).

The mechanical aspect of this project is to design an airworthy airframe which can capacitate the requirements for the solar energy harvesting and flight capability.

The main application of this model is to measure VOC gas concentration at different aerial altitudes, simultaneously. Data collected during the mission will be transmitted in real time to a central node for analysis. The system provides an effective 3D monitoring and can be used in a wide range of environmental applications such as agriculture, bushfires, mining studies, and zoology and botanical studies using a ubiquitous low cost technology.

The primary objective of this project is to make people aware of the fact, which the conventional energy sources are limited and that renewable energy must and can be used to solve future demand.

CHAPTER ONE

INTRODUCTION

1. INTRODUCTION

UAV (Unmanned Aerial Vehicle), commonly known as a drone, is an aircraft without a human pilot aboard. It can be either a drone (multiple rotors capable of vertical takeoff) or a glider (multiple rotors for horizontal takeoff). UAVs are a component of an unmanned aircraft system (UAS); which include a UAV, a ground-based controller, and a system of communications between the two. The flight of UAVs may operate with various degrees of autonomy: either under remote control by a human operator or autonomously by onboard computers. Compared to manned aircraft, UAVs were originally used for missions that are too dangerous for humans. While they originated mostly in military applications, their use is rapidly expanding to commercial, scientific, recreational, agricultural, and other applications, such as policing, peacekeeping, and surveillance, product deliveries, aerial photography, agriculture, and drone racing. Civilian UAVs now vastly outnumber military UAVs, with estimates of over a million sold by 2015, so they can be seen as an early commercial application of autonomous things, to be followed by the autonomous car and home robots.

In today's world, there are more than 11,000 unmanned aerial vehicles (UAVs) in service (or planned for future services) by the Military for various purposes. These vehicles can fly remotely as well as autonomously. In spite of their usage in various applications, they lack in performance because of power restrictions, which means they either have to land to refuel or to depend on another UAV to complete the task. Nowadays the ability to fly without using conventional fossil fuels is primarily focused in recent years, both in application point of view and scientific field since the major concerns are increasing global warming and a decreasing natural resources. Since then, the use of electric aircraft has been widespread but here the crucial issue is their high power consumption when compared with their limited energy storage capability, which leads to an endurance that can rarely exceed half an hour. Increasing the size of the battery or incorporating more batteries increases the weight of the plane, which affects the flight time of the UAV as it is inversely proportional. So, now, the ability to fly an aircraft to increase the endurance limit has been a key issue in both UAVs and civilian aviation. One of the possibilities to increase the flight time is by using unlimited solar energy through solar cells. These cells, by connecting them with

an electronic circuit, can provide sufficient power for motor and the electronics and, if in excess, it can also be stored in the battery; here the battery can be used as a buffer when flying in darkness or under clouds. Hence, the possible solution to enhance the endurance is by using solar powered aircraft driven by electric-based propulsion systems in which the power is supplied continuously throughout the day by the unlimited solar energy, which can eliminate fuel and also solve the limited energy storage capability problem.

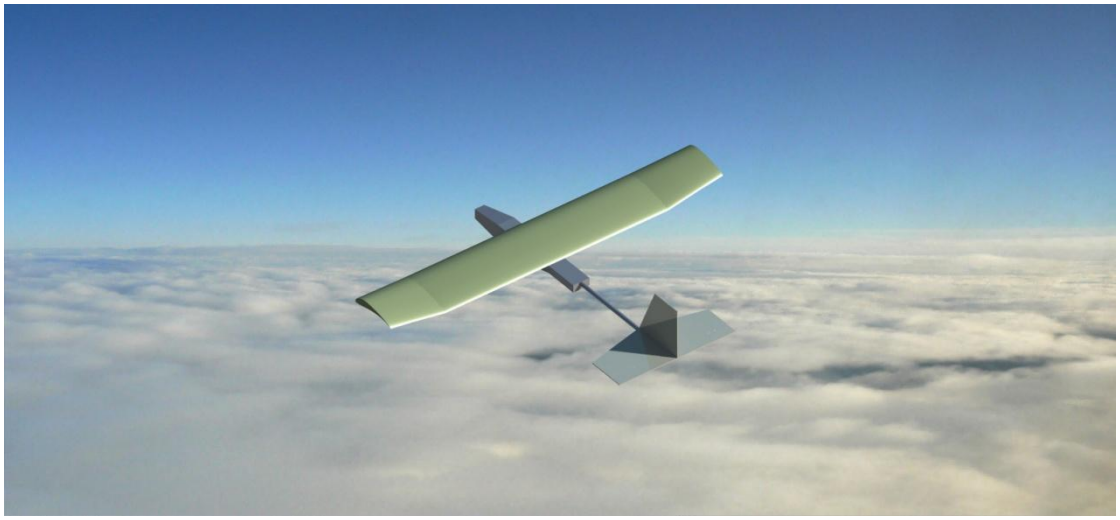

Fig. 1.1: Basic UAV (CAD model render)

Solar power is the cleanest energy in the world. Usages of solar energy are widespread in industry, commercial, and military applications. Every day, the sun gives off far more energy than we need to power everything on earth. Solar panels produce electricity by transforming the continuous flow of energy from the sun to electricity. No harmful emissions are released into the air when electricity is produced by solar panels. The photovoltaic process that transforms sunlight into electricity doesn't require any fuel and has no variable costs. The solar energy has unlimited reserves, hence can be used in aircraft as a primary source of power. The main principle is to make use of available unlimited solar energy by converting it into electricity through solar cells. When sunlight strikes the solar cell, the cell creates electrons and holes as charge carriers and, when a circuit is made, these free electrons pass through a certain load in order to recombine with the holes and, in this way, the current is generated. Here, by arranging solar cells in series on the top of the wing and then wrapping the entire wing with transparent material for the safety of solar cells

during flight. Cells are arranged in series to get the required voltage in order to safely charge the 3S battery; from there, the battery power is supplied to the motor for throttling during constant level flight. In this study, the aircraft was assumed to be a glider, which means it also stores the energy in the battery during the gliding period. In this way, both flying the plane by using solar energy alone and storing the energy in the battery in order to extend the flight time can be achieved. A solar-powered UAV could in principle stay overhead indefinitely as long as it had a proper energy-storage system to keep it flying at night. The design of the power management system for such aircraft is challenging due to possible rapid attitude changes during manoeuvres. It is also used to charge the battery, used as a backup source when sunlight is not sufficient to produce enough power. The most common form of the energy storage for the stand alone solar power system is battery technology. The basic functions of the battery management are to control the charge/discharge of the battery, to protect the battery from damage, to prolong the life of the battery, and to maintain the battery in a state to fulfil the functional requirements. The lithium-ion polymer battery is selected for this UAV application study.

Fig. 1.2: Real Life Glider Model.

Air pollution causes health effects and environmental problems. Typical air pollutants that cause immediate concern are PM2.5 and VOCs. Airborne particulate matter (PM) varies widely in its physical and chemical composition, source and particle size. PM10 particles (the fraction of particulates in air of very size < 10 μm) and PM2.5 particles (< 2.5 μm) are of major current concern, as they are small enough

to penetrate deep into the lungs and so potentially pose significant health risks. Larger particles meanwhile, are not readily inhaled, and are removed relatively efficiently from the air by sedimentation. The principal source of airborne PM10 and PM2.5 matter is road traffic emissions, particularly from diesel vehicles. HC (compounds of hydrogen and carbon only) belong to a larger group of chemicals known as volatile organic compounds (VOCs). They are produced by incomplete combustion of hydrocarbon fuels, and also by their evaporation. Assessment of air quality has been traditionally conducted by ground based monitoring, and more recently by manned aircrafts and satellites. However, performing fast, comprehensive data collection near pollution sources is not always feasible due to the complexity of sites, moving sources or physical barriers. Small Unmanned Aerial Vehicles (UAVs) equipped with different sensors have been introduced for air quality monitoring, as they can offer new approaches and research opportunities in air pollution and emission monitoring, as well as for studying atmospheric trends, such as climate change, while ensuring urban and industrial air safety.

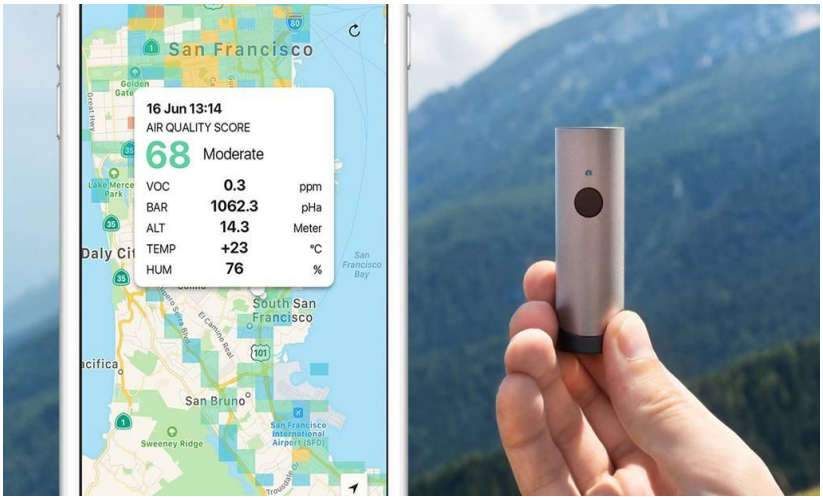

Fig. 1.3: Air Quality Analyser - AtmoTube

In our project, we plan to create a glider which runs on electric batteries which can be charged by supplying energy through mains as well as through the solar energy incident on it. This project adds a new dimension to air quality analysis. The UAV can be used to sample ambient air at different altitudes (1m to 50m). The throw of this project is towards sustainable development.

1.1 Problem Statement

To design, develop, fabricate and experimentally test a solar powered unmanned Ariel vehicle and use it for air quality analysis for a particular geographical area.

1.2 Objectives

- To design an air worthy and stable air frame.
- To use a hybrid system to power the aircraft that uses battery power as well as solar energy.
- To manufacture and validate the design by experimental testing and simulations.
- To use the model for air quality analysis.

1.3 Scope

The scope of our work includes monitoring the variations in endurance of our solar powered UAV model. Outdoor experiments were carried out at different environmental conditions of wind speeds, altitude and performance of the model in different scenarios was observed. The model was used to analyse air quality.

1.4 Methodology

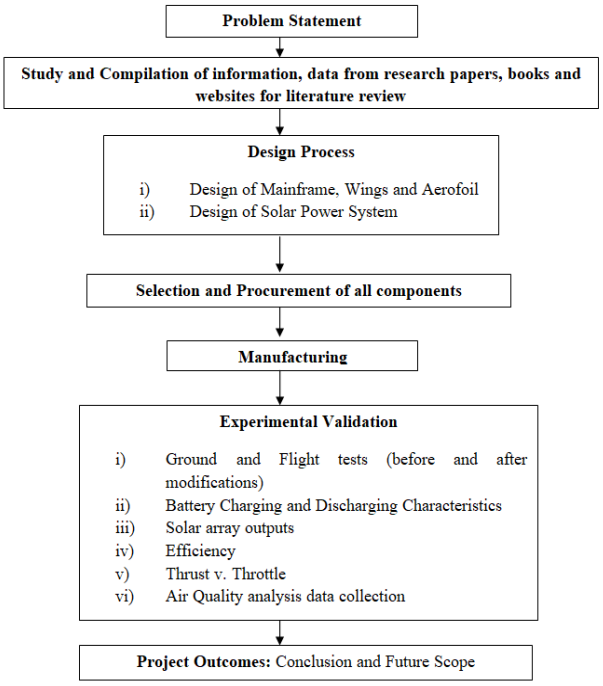

Fig. 1.4: Methodology

1.5 Organisation of Dissertation

- Introduction – The problem statement is defined, the objectives and scope for this project along with methodology is listed.
- Literature Review – Various research papers, books and websites have been referred and relevant literature has been mentioned.
- Design, Simulation and Manufacturing – The design process includes various analytical, arbitrary methods and softwares like CATIA, XFLR5 for CAD modelling and CFD processes. Manufacturing describes different effective methods.
- Experimental Validation – It includes the validation, experimental testing of design, power system and air quality measurement system and the results.
- Conclusion – It includes interpretation of the results of the entire UAV system obtained after experimental validation and testing of various sub-systems and future scope.

CHAPTER TWO

LITERATURE REVIEW

2. LITERATURE REVIEW

Aditya A Paranjape, et al [1], describes the flight mechanics of a micro aerial vehicle without a vertical tail, in an effort to reverse-engineer the agility of avian flight. The key to stability and control of such a tail-less aircraft lies in the ability to control the incidence angles and dihedral angles of both wings independently. The dihedral angles can be varied symmetrically on both wings to control aircraft speed independently of the angle of attack and flight path angle, while asymmetric dihedral can be used to control yaw in the absence of a vertical stabilizer. It is shown that wing dihedral angles alone can effectively regulate sideslip during rapid turns and generate a wide range of equilibrium turn rates while maintaining a constant flight speed and regulating sideslip.

S. Jashnani, et al [2] reveals that integrating solar energy into modern aircraft technology has been a topic of interest and has received a lot of attention from researchers over the last two decades. A few among the many potential applications of this technology are the possibility of continuous self sustained flight for purposes such as information relay, surveillance and monitoring. Possible applications of the Unmanned Aerial Vehicle (UAV) include military and classified surveillance flights where small aircrafts are difficult to be detected by radars. Scientific applications include ozone monitoring, and collection of data for weather and global warming studies. Commercial applications include aerial surveying, geological and topographical mapping, and communication links. Solar powered UAV can be employed in many of the above mentioned missions due to its cost effectiveness, environmental efficiency, and also because it is capable of long endurance flight and does not require much maintenance. The assumed value of the solar panel area along with the total solar available energy per meter squared, are used to calculate the total available solar energy. This energy when divided by the total time of the day gives the average available solar power over the day. This power will be compared with the solar power required to generate the required thrust and operate aircraft accessories, and hence the assumed value for the solar panel area will be changed till convergence. Practically, the solar panels can cover up to about 90% of the wing width and span. Thus, from the assumed value of the solar panel area, the wing area can be evaluated. Select an airfoil section and get the lift and drag polar curves for this airfoil. The angle

of attack that provides a maximum lift-to-drag ratio is selected as the mounting angle of the wing. With the known propulsive power, the required power output from the battery is estimated by dividing the propulsive power by the efficiency of the propulsion and power system train till the battery. Also, the required power to operate the payload and avionics has to be added to this value. The energy-time management of the battery is simulated by estimating energy in and out of the battery at each hour, starting at takeoff condition. Thus, the initially stored energy is added to the collected energy at the first hour of flight. Then, the energy required, for the propeller and accessories, is subtracted to give the remaining stored energy in the battery at the first hour of flight. Similarly, at the next hours, the available energy in the battery is estimated. The required solar panel area at sea level is greater than that at 5 km. This is because for altitudes above 2.5 km, the effect of cloud is negligible. However, as the altitude increases, the air density and pressure decrease. This requires more area to generate enough lift to sustain the weight of the aircraft. This causes the panel area to increase with altitude as well as with the payload mass.

Stanley R. Herwitz [3], UAVs are expected to play an expanded role, complementary to that of satellites and conventionally piloted aircraft, for agricultural support. Beyond that, loitering UAVs may provide image support to user communities in disaster relief, fire management, and homeland security. Unmanned aerial vehicle (UAV) capabilities are evolving rapidly, from both technical and regulatory standpoints. It is likely that these platforms will begin to offer new alternatives for agricultural and other users needing high spatial resolution digital imagery acquired and delivered in near-real time. The purpose of this study is to demonstrate safe operation of a UAV for remote sensing in the U.S. National Airspace System (NAS), and to acquire, enhance, and distribute high-spatial resolution digital imagery for commercial agricultural decision support.

Philipp Oettershagen, et al [4], states that when carefully designed, solar-electrically powered fixed wing Unmanned Aerial Vehicles (UAVs) exhibit significant increase in flight endurance over purely-electric or even gas-powered aerial vehicles. Given suitable environmental conditions, a solar-powered UAV stores excess solar energy gathered during the day in its batteries, which may then power the aircraft through the night and, potentially, subsequent day-night cycles. Long-endurance capability,

especially in the extreme form of continuous multi-day flight, or perpetual endurance, is particularly interesting for applications such as large-scale mapping, observation, or telecommunication relay. Such functionalities may be applied to Search-And-Rescue (SAR) missions, industrial or agricultural inspection, meteorological surveys, border patrol and more.

Prof. E.G. Tulapurkara, et al [5], indicate that the horizontal and vertical tails are designed to provide stability; the movable surfaces on tails namely elevator and rudder provide control. The complete design of tail surfaces requires information on (a) location of the centre of gravity (C.G.) of airplane, (b) shift in C.G. location during flight and (c) the desirable level of stability. However, to obtain the C.G. location, the weights of horizontal and vertical tails are needed which depend on their size. i) Nearly 70% of the airplanes have conventional tail i.e. horizontal tail is behind the wing and located on the fuselage. ii) Nearly 25% of the airplanes have T-tail .The T-tail configuration has the following advantages. a) The horizontal tail acts as an end plate on the vertical tail. This reduces the adverse effect of finite aspect ratio on the vertical tail and increases its slope of lift curve. b) Horizontal tail is away from wing wake. The effect of propeller slip stream or down wash due to jet engine exhaust is minimal. The disadvantage of the T-tail is that (a) the vertical tail structure is heavier and (b) at high angles of attack, beyond stall angle of the wing, the tail is in the wake of the wing. The latter condition is avoided with the help of stall warming devices. The airplanes with engines mounted on rear fuselage invariably have T-tails. iii) Cruciform tail: The horizontal tail is located in the middle of vertical tail. This arrangement is a compromise between conventional and T-tail. iv) H-tail and Triple tail: In these configurations the vertical tail is in two or three parts. This helps in reducing the height of the vertical tail. It also provides some end plate effect on the horizontal tail. v) V-Tail: In this configuration the horizontal and vertical tail surfaces are combined. However, there is no significant reduction in total tail area. On the other hand, this configuration results in undesirable coupling of longitudinal and lateral motions of the airplane. The aspect ratio, taper ratio, sweep, airfoil section and incidence of the horizontal tail are selected based on the following considerations. It may be pointed out that the shapes of the horizontal tail and vertical tail are like that of a wing. In such shapes, especially for subsonic airplanes, the span is much larger than the chord and in

turn the chord is much larger than the airfoil thickness. For example, in case of subsonic airplanes the span is 6 to 10 times the average chord and the average chord in turn is 6 to 10 times the thickness of the airfoil. The flow past such shapes (wings) can be obtained in two stages. First by studying the flow past the airfoil, then the flow past the wing is obtained by applying corrections for the effects of aspect ratio, taper ratio and sweep. The elevator and rudder have deflections on both sides of the undeflected positions. Hence, horizontal and vertical tails invariably have symmetric airfoil section. National Advisory Commilis for Aeronautica (NACA) generated a large amount of data on the aerodynamic characteristics (C_l vs. α, α vs. C_d and C_d vs. C_l) at different Reynolds numbers, flap settings etc. for NACA 0009 and NACA 0012 airfoils. Hence, these airfoils are commonly used for tails of airplanes flying at low and medium subsonic Mach numbers. For airplane flying at high subsonic Mach numbers, the drag divergence Mach number of the tail should be higher than that of the wing. A symmetrical airfoil with (t/c) of 90 % of the (t/c) of the wing can be a rough guideline for preliminary design purpose.

Grant E. Carichner, Leland M. Nicolai [20], examine a modern conceptual design of both airships and hybrids and features nine behind-the-scenes case studies. It will benefit graduate and upper-level undergraduate students as well as practicing engineers. The authors address the conceptual design phase comprehensively, for both civil and military airships, from initial consideration of user needs, material selection, and structural arrangement to the decision to iterate the design one more time. The book is the only available source of design instruction on single-lobe airships, multiple-lobe hybrid airships, and balloon configurations; on solar and gasoline-powered airship systems, human-powered aircraft, and no-power aircraft; and on estimates of airship/ hybrid aerodynamics, performance, propeller selection and empty weight. The book features numerous examples, including designs for airships, hybrid airships, and a high-altitude balloon; nine case studies, including SR-71, X-35B, B-777, Honda Jet, Hybrid Airship, Daedalus, Cessna 172, T-46A, and hang gliders; and full-colour photographs of many airships and aircraft.

Senator John H. Glenn, Jr. in ‘NASA’s Let It Glide’ [23], refers to aerodynamics as a study of interaction between air and objects moving through it. An airplane flies as a result of the imbalance of four forces—thrust, drag, lift, and weight. A force is a push

or a pull on an object. The airplane's engines generate a force called thrust which moves the plane forward. As the airplane moves forward, the air around the plane creates a resistive force known as drag. The same force can be felt when you stick your arm out of the window of a moving car. As air flows over and under the airplane's wings, they generate an upward force called lift. Airplanes take off and land into the wind to maximize air flow to create the most lift. When enough lift is generated to overcome the airplane's weight, the downward (opposite) force of the airplane's mass caused by gravity, the airplane will take off. Lift is the most complex of the four forces and can be affected by changing one or more features of an aircraft's wings: geometry — the wing's shape and area the length and width. You can vary the distance from the front edge to the back edge of the wing, called the chord, as well as vary the length of the wing. Long thin wings will generate less drag than short thick ones with the same area. Thickness — the longest distance through the wing from the top surface to the bottom surface airfoil shape — the cross-sectional shape of the wing. This shape can be changed to affect lift by varying the degree of curve of the top and bottom surfaces, known as camber. Airfoils are designed with precise camber to keep air flowing closely over the wing and turn the air downward to create lift. Newton's third law of motion states for every action there is an equal and opposite reaction. Because the wings push the air downward, the air pushes the airplane upward. Changing camber can also speed up air moving along the wing's top surface. Bernoulli's principle states that an increase in the speed of air causes a decrease in pressure. The wing will generate an additional lift as the higher pressure air below the wing pushes it up into the lower pressure air above a cambered airfoil showing Bernoulli's principle. Angle of attack — the angle of the airfoil compared to the direction of the oncoming air. Increasing angle of attack causes more air to turn downward, creating additional lift. Too much of an angle, however, will causes the wing to lose lift and stall. Without lift, gravity takes over and the plane falls toward Earth. Sweep — the angle between a line perpendicular to an airplane's fuselage and the leading edge of its wing. Swept-back wings create less drag than straight wings. It is more noticeable at higher speeds. Gliders are a special type of flying vehicles. Since a glider cannot continue to add thrust on its own to move forward, the drag generated gradually slows it down. As less air flows over the wing, the glider loses lift and descends to the ground. The ratio of the horizontal distance travelled to the change in

vertical height as the glider falls is called the glide slope. Gliders are designed to maximize glide slope to provide the longest flight.

Alejandro Diaz Puebla, et al [24], divulges the main aim of the work carried out in the actuator sizing was to provide a general overview of the new actuators that are currently being implemented. These actuators are powered by an electric motor, due to the present tendency of the development of MEA concept. It can be considered a first step into a preliminary sizing model of EHAs and EMAs, although at this point more research is needed. It is necessary for the utilization of the model or of any other model based on scaling laws- to have an updated and detailed actuator data table with dimensions and parameter values of existing flight control surface actuators. It would be also necessary a more detailed model of the sizing of both types of actuators in order to achieve a closest solution to real values beyond preliminary design models. Furthermore, throughout the development of this thesis it has been noticed the endless possibilities and applications that parametric CAD design can have in the field of engineering. The parametric design has been the key point of the flaps integration in RAPID to allow the user to choose any control surface configuration with almost no effort or previous CAD design knowledge. Moreover, the implementation of automatic instantiations and procedures has also been an essential condition to achieve the objectives sought. Thanks to the automation the users are not only capable to instantiate one model, but to create a whole wing configuration and implement instantly any possible change. The use of Knowledge Pattern and UDFs in the instantiation process involves a considerable decrease in the complexity of the user interface, as by this instantiation procedure the user interface is only composed by the parameters needed to define the model. To conclude, flexible flight control surface integration in RAPID has been developed, proving the potential of CATIA GSD and Knowledge Pattern workbenches as engineering design tools.

Ideen Sadrehaghighi, in ‘Aerodynamic Design & Optimization’ [25], states the optimization algorithms used with the direct design method are mainly the gradient based methods and the stochastic (random) algorithms. Gradient-based methods rely on derivative information for all the objectives and all the constraints to determine the optimization search direction. These methods start with a single design point and use the local gradient of the objective function with respect to changes in the design

variables to determine a search direction by using methods such as the steepest descent method, conjugate gradient method, quasi-Newton techniques, or adjoin formulations. These methods are efficient and can find a true optimum as long as the objective function is differentiable and convex. However, the optimization process can sometimes lead to a local, not necessarily a global, optimum close to the starting point. Furthermore, such computations can easily get bogged down when many constraints are considered. Genetic Algorithms and Evolutionary algorithms are typical stochastic optimization algorithms. These methods are robust optimization algorithms that can cope with noisy, multimodal functions, but are also computationally expensive in terms of the necessary number of flow analyses required for convergence. They start with multiple points sprinkled over the entire design space and search for true optimums based on the objective function instead of the local gradient information by using selection, recombination, and mutation operations. When implementing multidisciplinary design optimization in the automotive industry, there are several questions related to the subjects studied that need to be answered. Simulations associated to structural applications within the automotive industry are computationally expensive, which motivate the use of meta-model-based design optimization. It was concluded that which types of design of experiments, meta-models, and optimization methods that could be appropriate for automotive applications. Further on, an MDO method must be chosen. It must be determined whether a single or multi-level method should be used. Using a multi-level method increases the complexity of the optimization process considerably compared to using a single-level method. Therefore, in order to motivate the use of a multi-level method, the benefits must be greater than cost.

Amertha A. and Krishnakumaram, et al [7], referred to the solar power system used in Unmanned Aircraft Systems (UAS). This paper deals with the design consideration and development of solar power system capable of providing endurance for longer time than conventional UAS's. The Unmanned Aircraft Systems (UAS) is used for many applications these days, both in military and civil applications. The use of UAS is increasing rapidly due to the reduced production and operating cost compared to the large conventional aircraft. The problem faced by the most UAS is their minimum endurance (non-stop time of flight). This problem can be overcome by using solar

energy in the UAS, called solar powered UAS. Solar energy is readily available in India for most part of the year and can be utilized to power the aircraft and its sub systems. They can have long endurance with a backup battery power. The power management system mainly consists of power estimation, the maximum power point tracking (MPPT), battery management system (BMS), and the power conversion stages. The MPPT stage attempts to obtain the maximum power available from the solar cell panels. The battery management stage (BMS) monitors and controls the charge and discharge processes of the Li-Ion polymer battery modules. The simulation is done MATLAB/SIMULINK of version (R2012a).

Karthik Reddy, et al [8], described the various design aspects of the solar-powered UAV. This paper aims to encourage research on renewable energy sources for aviation considering the basic challenges for a solar-powered aircraft: geographical area of operation, energy collection and storage, payload and design parameters. Hence, a plane is designed for a certain load, including the payload and its mass, and is analyzed in various aspects. Besides, the design is optimized starting from airfoil to complete structure for better performance. We referred this paper for the estimation of the number of solar cells required and its arrangement on the wing.

Mohd. Rizwan Sirajuddin Shaikh, et al [9] mentioned the conversion of sunlight to direct current (DC) electricity by PV cells. Charge Controller work as control the power from solar panel which reverses back to solar panel get cause of panel damage. Battery System act as storage of electric power is used when sunlight not available (i.e. night). This system is connected to inverter to convert Direct Current (DC) into Alternating Current (AC). The cells converted solar radiation directly into electricity. It consist various kinds of semiconductor materials. It has two types: positive charge and negative charge. This cell technology is used to design solar cells with low cost as well as high conversion efficiency. When the cell absorbed photons from sunlight, electrons are knocked free from silicon atoms and are drawn off by a grid of metal conductors, pressure a flow of electric direct current. Solar cell PV made up of many chemicals.

S. P. Sukhatme and J. K. Nayak, [10], say that solar cells are used for photovoltaic conversion states that when solar radiations fall on these devices, it is converted

directly into DC electricity. The principle advantage associated with solar cells are that they have no moving parts, require little maintenance and work quite satisfactorily with beam and diffused radiation. Also they are readily adapted for varying power requirements because a cell is like a building block. The main factors limiting its use are that they are still costly and that there is very little economy associated with magnitude of power generated in an installation.

However significant developments have taken place in the last few years. New types of cells have been developed, innovative manufacturing processes introduced, conversion efficiencies of existing types increased, costs reduced and the volume of production increased. The annual world production of photovoltaic devices in 2006 was about 2500MWp. The corresponding production in India was about 90MWp with a significant amount being exported. As a result of above developments , solar cells are being used extensively in many consumer products and appliances and it is possible that in future they may become one of the important sources of energy for providing local amount of energy, particularly in rural and remote locations.

Principle of working: The first solar cells were made in the fifties from single silicon cell. Even today silicon is mostly used for making solar cells. Single crystal silicon cells are thin wafers about 0.250mm thickness sliced from a single crystal of p-type doped silicon. A shallow junction is formed at one end by diffusion of n-type impurity. Metal contacts are attached to the front and back side of the cells. On the front side the contact is in the form of metal grid with fingers to permit the sunlight to go through, while on the back side the contact completely covers the surface. Manufacturers have their own technique for producing inexpensive and reliable contacts. Generally for front screen printing of paste consisting of 70% silver, an organic binder and sintered glass is done. For the back, a paste containing aluminum is screen printed. The cells are places in a furnace at about 700 C so that the metals in the paste diffuse at the front and back to make the contacts with silicon. An anti reflection coating of silicon nitride or titanium oxide having a thickness of about 0.1 micrometer is applied on the top surface to complete the cell. A typical cell develops a voltage of 0.5 to 0.7 V and a current density of 20-40 mA/cm^2. In order to obtain higher voltages and currents, individual cells are fixed side by side on a suitable backup board and connected in series and parallel to form a module. The cells are encapsulated in thin transparent

material in order to protect them from environment and to support the module. A number of modules are interconnected to form an array. Earlier the cells used to be circular in shape. Now they are often rectangular in shape resulting in more compact modules. Apart from single crystal silicon, cells are also produced from multi-crystal silicon and amorphous silicon.

Working principle of solar cell:

1. Creation of pairs of positive and negative charges in the solar cells by absorbed solar radiations

2. Separation of positive and negative charges by potential gradient within the cell.

For the first step to occur, the cell must be made of the material which can absorb the energy associated with photons in the light. The energy (E) of a photon is related to the wavelength (λ) by the equation, $E = h*c/\lambda$

h = Planck's constant = 6.62×10^{-27} erg-s

c = Velocity of light= 3×10^{8} m/s.

Substituting these values we get,

$E = 1.24/\lambda$, where E is in electron-volts and λ is in μm.

The materials suitable for absorbing the energy of the photons are semiconductors like silicon, cadmium telluride, gallium arsenide etc. in a semiconductor the electrons occupy one of the two energy bands , the valence band and the conductance band . The valence band has electrons at a lower energy level and is fully occupied while the conductance band has electrons at a higher energy level and is not fully occupied. The difference between the minimum and the maximum energy levels is called the band gap energy E_g.photons of the energy E greater than the band gap energy E_g are absorbed in the cell material and excite some electrons. These electrons jump across the band gap from valence band to conductance band leaving behind holes in the valence bands. Thus electron- holes pair are created.

Parvathy Rajendran, et al [11], states that the two main functions of a battery is to receive charge and discharge. Therefore, charging and discharging play a major role in

the performance and life span of a battery. Thus, identifying the optimum operating temperature, required current and its corresponding flow rate for the battery is essential to maximize any UAV capabilities. The charging duration to full capacity of this LiPo cell is maintained at average value of 2 hours approximately which is supposed to be half an hour theoretically at high charging rate. Hence, a high charging rate still requires a considerable amount of time to charge to full capacity completely. So, it is best to avoid charging a battery at charging rate beyond 1 C. Therefore, for the solar module installed in solar-powered UAV developed by Aircraft Design Group, Cranfield University was designed to charge the battery pack at a nominal or maximum rate of 0.129 C and 0.155 C correspondingly. Thus, the solar module requires roughly 5.73 hours on nominal charging rate on 30 °C operating temperature to fully charge capacity level instead of 5.54 hours theoretical predicted. The battery pack will then discharge at cruise flight roughly about 0.071 C to a maximum of 1.685 C if required. If the battery pack is not charged, during cruise flight the battery capacity will deplete completely at about 6.51 hours for the same operating temperature, in contrast to the 6.48 hours based on the theoretical prediction. The optimum temperature for charging and discharging the LiPo battery is slightly more than room temperature. This clearly states that the usage of LiPo batteries for operation at high altitudes and/or extreme temperatures without an additional heating or cooling system for these battery packs is not favourable. Thus, it is best to charge at low charging rate and high operating temperature to store the most capacity in a battery.

Yevgen Barsukov, et al [12], defined a Current Bypass - Simple implementation of cell-balancing includes a FET placed in parallel with each cell and controlled by a comparator for simple voltage based algorithms that turn-on the bypass FETs during the onset of voltage differences, or by microcontroller for more complex and effective algorithms that can work continuously regardless of variations of voltage differences. Main choice here is to use FETs that are integrated in the balancing controller IC and typically have by-pass currents from 9 to 2 mA (depending on the choice of the external resistors), or to use external FETs with by-pass capability that can be freely tailored to particular application needs. In Li-ion batteries which have very low self discharge and therefore accumulative unbalance per cycle is usually less than 0.1%,

bypass current of internal FETs is sufficient to keep the pack continuously balanced. In other chemistries where self-discharge is much higher and therefore differences in self-discharge rates between the cells results in higher SOC differences per cycle, higher rates might be needed. Charge Redistribution - The disadvantage of current by-pass approach is that the energy of the by-passed charge is wasted. While this can be acceptable during charge while system is connected to power grid, during actual usage of the battery in portable applications every mille-Watt-hour is precious. This asks for a possibility to have a cell-balancing approach that would allow draining the "high" cells to the bottom using most efficient way. The ultimate approach for this is to use a pack that has no serially connected cells at all. The step-up converter would then assure that device will obtain sufficient voltage. This way energy waste from cell-balancing is completely eliminated. The trade-off however is lower efficiency of the power supply, as well as its increased size and complexity. Other solutions can include circuits that allow transferring energy from high cells to low cells rather than burning it in a by-pass resistor. Charge Shuttles is a simple approach to redistribute the energy between the cells is to connect a capacitor first to higher voltage cell, than to lower voltage cell, More complicated implementations allow the connection of not only two nearby cells, but also cells for far away in the stack for faster The main problem with this method is that significant energy losses occur during capacitors charging, as maximal efficiency of this process is 50%. Another problem is that high voltage differences between the unbalanced cells exist only in highly discharged state. Because this method transfer rate is proportional to voltage differences, it only becomes efficient near the end of discharge so total amount of unbalance that can be removed during one cycle is low. Inductive Converters is a cell-balancing method that is free from the disadvantage of small voltage differences between cells decreasing the balancing rate is implemented by transferring pack energy into single cell by directing pack current through a transformer which is switched to one of the cells that needs additional charge. However, efficiency of such converter is limited, and the need to use a transformer results in increased price and size of the overall solution. So far no commercial implementations of such system in portable devices have been successful. Probably area where it could be more practical are high-power systems such as EV and hybrid vehicles. Regardless of particular hardware implementation, there is always a decision to be made, when to turn ON bypass switch or when to engage the energy

exchange circuit to particular cell. Different algorithms of making this decision are reviewed below. For simplicity we will refer to the case of current bypass because transfer of the logic to other balancing schemes is trivial. Cell voltage based- Simplest algorithm is based on voltage difference between the cells. If difference exceeds predefined threshold, bypass is engaged. To resolve several problems of this simple method, more complicated modifications can be implemented if microcontroller is used to execute the algorithm:

• Balancing during charge only is used to save energy in portable applications.

• Balancing at high states of charge only is used to decrease the effect on SOC balancing that can come from impedance unbalance.

• Simultaneous multi-cell balancing makes decision on which cells have to be bypassed under considerations of the entire pack and not only neighbouring cells as it is the case with comparator-based solutions. One of the advanced implementation of voltage-based algorithms using all above optimizations is used in bq2084 battery fuel gauge.

Bisht DS, Tiwari S, et al [16], mention that the ground and vertical profiles of particulate matter (PM) were mapped as part of a pilot study using a Tethered balloon within the lower troposphere (1000 m) during the foggy episodes in the winter season of 2015–16 in New Delhi, India. Measurements of black carbon (BC) aerosol and PM < 2.5 and 10 μm ($PM_{2.5}$ & PM_{10} respectively) concentrations and their associated particulate optical properties along with meteorological parameters were made. The mean concentrations of $PM_{2.5}$, PM_{10}, $BC_{370\ nm,}$ and $BC_{880\ nm}$ were observed to be 146.8 ± 42.1, 245.4 ± 65.4, 30.3 ± 12.2, and $24.1 \pm 10.3\ \mu g\ m^{-3}$, respectively. The mean value of $PM_{2.5}$ was ~ 12 times higher than the annual US-EPA air quality standard. The fraction of BC in $PM_{2.5}$ that contributed to absorption in the shorter visible wavelengths ($BC_{370\ nm}$) was ~ 21%. Compared to clear days, the ground level mass concentrations of $PM_{2.5}$ and $BC_{370\ nm}$ particles were substantially increased (59% and 24%, respectively) during the foggy episode. The aerosol light extinction coefficient (σ_{ext}) value was much higher (mean: 610 Mm^{-1}) during the lower visibility (foggy) condition. Higher concentrations of $PM_{2.5}$ ($89\ \mu g\ m^{-3}$) and longer visible wavelength absorbing $BC_{880\ nm}$ ($25.7\ \mu g\ m^{-3}$) particles were observed up to 200 m.

The $BC_{880\ nm}$ and $PM_{2.5}$ aerosol concentrations near boundary layer (1 km) were significantly higher (~ 1.9 and 12 $\mu g\ m^{-3}$), respectively. The BC (i.e. BC_{tot}) aerosol direct radiative forcing (DRF) values were estimated at the top of the atmosphere (TOA), surface (SFC), and atmosphere (ATM) and its resultant forcing were -75.5 Wm^{-2} at SFC indicating the cooling effect at the surface. A positive value (20.9 Wm^{-2}) of BC aerosol DRF at TOA indicated the warming effect at the top of the atmosphere over the study region. The net DRF value due to BC aerosol was positive (96.4 Wm^{-2}) indicating a net warming effect in the atmosphere. The contribution of fossil and biomass fuels to the observed BC aerosol DRF values was ~78% and ~22%, respectively. The higher mean atmospheric heating rate (2.71 K/day) by BC aerosol in the winter season would probably strengthen the temperature inversion leading to poor dispersion and affecting the formation of clouds. Serious detrimental impacts on regional climate due to the high concentrations of BC and PM (especially $PM_{2.5}$) aerosol are likely based on this study and suggest the need for immediate, stringent measures to improve the regional air quality in the northern India.

Stephen W. Moore, et al [17] states that Lithium Ion and Lithium Polymer battery chemistries cannot be overcharged without damaging active materials. The electrolyte breakdown voltage is precariously close to the fully charged terminal voltage, typically in the range of 4.1 to 4.3 volts/cell. Therefore, careful monitoring and controls must be implemented to avoid any single cell from experiencing an overvoltage due to excessive charging. Single lithium-based cells require monitoring so that cell voltage does not exceed predefined limits of the chemistry. Series connected lithium cells pose a more complex problem: each cell in the string must be monitored and controlled. Even though the pack voltage may appear to be within acceptable limits, one cell of the series string may be experiencing damaging voltage due to cell-to-cell imbalances. Traditionally, cell-to-cell imbalances in lead-acid batteries have been solved by controlled overcharging. Lead acid batteries can be brought into overcharge conditions without permanent cell damage, as the excess energy is released by gassing. This gassing mechanism is the natural method for balancing a series string of lead acid battery cells. Other chemistries, such as NiMH, exhibit similar natural cell-to-cell balancing mechanisms. Electric vehicle applications can benefit from cell balancing devices, especially for lithium-based battery

chemistries. Since battery pack charging is limited by any one single cell reaching its end-of-charge voltage (4.1 V to 4.3 V), it is useful to control high voltage cells until the lower voltage cells catch up. This way, each cell can be charged to its end-of-charge voltage. Several cell-balancing methods are suitable for EV applications. Charge shunting methods work well but are limited by the amount of current that must be dissipated. The shared transformer method is applicable, but it is costly in terms of magnetic and parts count. The dissipative method is applicable, and is the most cost effective. Charge shuttling methods would be prohibitively expensive due to the switches required to handle the large peak capacitor charging currents. Hybrid electric vehicle applications typically feature regenerative braking, battery charging and electric motoring. These features put high demands on the battery pack for both charging and discharging. The battery pack is usually not kept in a fully charged condition; rather it is marginally charged, leaving room at the top for charge acceptance. Thus, charge shunting is not an applicable solution. Since some HEV designs features battery packs significantly smaller than their EV counterparts, charge shuttling methods become more attractive with smaller peak switch currents. However, the amount of energy dissipated in capacitor ESR and switching losses may not justify the increased complexity and expense. The dissipative method is effective without the complexity and expense. However, the algorithm development is significantly more involved. Cell balancing utilizing energy conversion devices employ inductors or transformers to move energy from a cell or group of cells to another cell or group of cells.

State of air in India: WHO reports 2018 reports that India is the home to 7 out of top 10 most polluted cities based on the amount of particulate matter under 2.5 micrograms found in every cubic meter of air. These cities are Kanpur, Faridabad, Varanasi, Gaya, Patna, Delhi, Lucknow, Agra, Muzaffarpur, Srinagar, Gurgaon, Jaipur, Patiala and Jodhpur. The centre formulated National Clean Air Programme (NCAP) to fight menace through long term strategy. It set the target to reduce 35% of the pollution in three years and 50% in the next 5 years for 100 identified cities.

Environment Ministry of government of India launched National Clean Air Programme (NCAP): The centre recently launched NCAP. The overall objective of this programme includes comprehensive mitigation actions for prevention, control and abatement of air pollution. It also aims to augment the air quality monitoring network

across the country and strengthen the awareness and capacity building activities. Also city specific plans are being formulated fro 102 non-attainment cities that are considered to have air quality worse than the National ambient Air Quality Standards. It proposes a tentative national target of 20%-30%reduction in pm2.5 and pm10 concentrations till 2024 with 2017 as the base year.

The Central Pollution Control Board (CPCB) is executing a nationwide program of ambient air quality monitoring known as National Air Quality Measurement Program. The network consists of 731 operating stations covering 312 cities in 29 states and 6 union territories. Under NAMP, following 4 air pollutants are indentified for regular monitoring at all locations:

1. Sulfur dioxide
2. Oxides of nitrogen
3. Respirable suspended particulate matter
4. Fine particulate matters.

The monitoring of the meteorological parameters such as wind speed and wind direction, relative humidity and temperature were also integrated with the monitoring of air quality. The monitoring is being carried out with the help of CPCB, SPCB, Pollution control committees, National Environmental Engineering Research Institute (NEERI) Nagpur.

NITI Aayog: Breathe India is a 15 point formula to combat air pollution proposed by NITI Aayog. It has sited WHO report to state Kanpur, Faridabad, Gaya, Varanasi and Patna are most polluted cities in the world. The plan seeks “concerted action from all levels of the governance”. The 15 point formula includes measures like replacing all petrol-diesel vehicles in use at government offices by electric and hybrid vehicles, streamlining power plants, encouraging solar panels in the roof tops and feebat scheme. It says that the government should increase the focus on electric and hybrid vehicles for central government use and some public facilities. It favored setting up smog free towers in the cities for providing quick relief from sudden spike in air pollution. it has called for implementing a large scale feebate program beginning 2020. A feebat is the policy that entails levying a surcharge on inefficient or polluting vehicles and giving a rebate on efficient ones.

World air quality report 2018 states India dominates the tops of the list. It asserted that 7 of the world's top ten cities with worst air quality are in India. The national ambient air quality standards define the permissible limit for concentration of pm2.5 at 40µg/m^3, on the other hand WHO defines them at 10µg/m^3.

Sarath K. Guttikonda, et al [15], mentioned various aspects regarding air quality monitoring in Indian cities, sources of air pollution in Indian cities, health impacts of outdoor air pollution in India, review of air quality management options at the national and urban scale is mentioned. An overview of the emission sources and control options for better air quality in Indian cities, with a particular focus on interventions like urban public transportation facilities; travel demand management; emission regulations for power plants; clean technology for brick kilns; management of road dust; and waste management to control open waste burning. Also included is a broader discussion on key institutional measures, like public awareness and scientific studies, necessary for building an effective air quality management plan in Indian cities is available from this paper. We used this data to study patterns of air pollution in major Indian cities and their air quality indices.

Polly E. Langa, et al [18] describes that air quality monitoring networks offer the potential to visualise and quantify long-term trends over large regions through aggregation of data from multiple monitoring sites. However, analysis of roadside monitoring site data from the London network suggests caution is required when averaging data from a monitoring network containing time series of variable duration. Movement, opening and closing of monitoring sites introduce biases into the average trend, resulting in a misleading view of the changes in air quality. Techniques were developed with the aim of identifying and mitigating these influences to robustly represent the true long term trend. In particular, a method involving the calculation of a change in concentration using rolling window regression was developed as an effective alternative to simple averaging. This technique was demonstrated to estimate the true trend in pollutant concentration with far greater accuracy than the simple average trend when applied to a set of time series of disparate lengths. The ability to use multiple time series of differing lengths in trend analysis offers potential advantages for air quality and environmental monitoring applications, as well as time series analysis in other fields. An important advantage of the technique is that it

maximises the use of the information available and is suited to situations where a large number of monitoring sites may not be available but where an aggregate view of overall changes in concentrations is still valuable.

In National Air Quality Index - Journal for Control of Urban Pollution Series (CPUS), [31] the CPCB took initiative for developing a national Air Quality Index (AQI) for Indian cities. AQI is a tool to disseminate information on air quality in qualitative terms (e.g. good, satisfactory and poor) as well as its associated likely health impacts. An expert group comprising medical professionals, air quality experts, academia, NGOs, and SPCBs developed National AQI. Necessary technical information was provided by IIT Kanpur. The draft AQI was launched in October 2014 for seeking public comments. It was also circulated to States Governments, Pollution Control Boards, concerned Central Government Ministries and premier research institutes for inputs. Comments received were examined by the Expert Group and a National AQI scheme was finalized, which is presented in this report. There are six AQI categories, namely good, satisfactory, moderately polluted, Poor, Very Poor, and Severe. The AQI considers eight pollutants for which short-term (up to 24-hourly averaging period) standards are prescribed, however, AQI can be calculated if monitoring data are available for minimum three pollutants of which one should necessarily be PM 2.5 or PM 10 . Based on the measured ambient concentrations, corresponding standards and likely health impact, a sub-index is calculated for each of these pollutants. The worst sub-index reflects overall AQI.

Applications of Air Quality Index:

The following six objectives that are served by an AQI:

1. Resource Allocation: To assist administrators in allocating funds and determining priorities. Enable evaluation of trade-offs involved in alternative air pollution control strategies.

2. Ranking of Locations: To assist in comparing air quality conditions at different locations/cities. Thus, pointing out areas and frequencies of potential hazards.

3. Enforcement of Standards: To determine extent to which the legislative standards and existing criteria are being adhered. Also helps in identifying faulty standards and inadequate monitoring programs.

4. Trend Analysis: To determine change in air quality (degradation or improvement) that has occurred over a specified period. This enables forecasting of air quality (i.e. tracking the behaviour of pollutants in air) and plan pollution control measures.

5. Public Information: To inform the public about environmental conditions (state of environment). It is useful for people who suffer from illness aggravated or caused by air pollution. Thus, it enables them to modify their daily activities at times when they are informed of high pollution levels.

6. Scientific Research: As a means for reducing a large set of data to a comprehendible form that gives better insight to the researcher while conducting a study of some environmental phenomena. This enables more objective determination of the contribution of individual pollutants and sources to overall air quality. Such tools become more useful when used in conjunction with other sources such as local emission surveys.

CHAPTER THREE

DESIGN PROCESS

AND

SIMULATION

3. DESIGN PROCESS AND SIMULATION

3.1. Design of Aircraft model

3.1.1. Design Load Derivations

The aircraft is subject to forces such as lift, drag, thrust and weight. We focused on designing for maximum lift and for a weight of 4.5 to 5 kg.

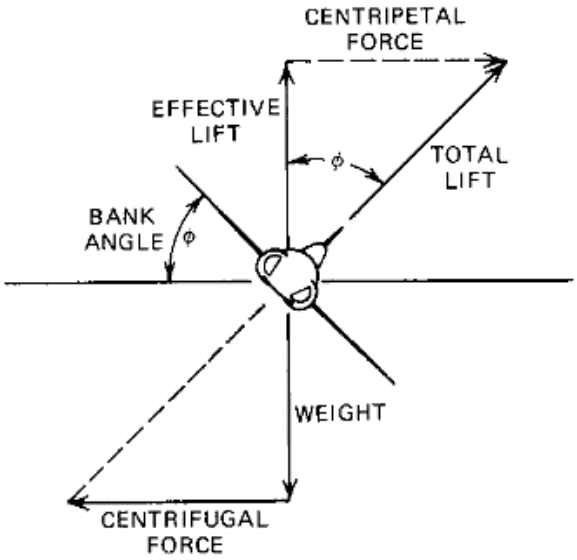

Fig. 3.1 Aircraft Forces in a Level

Additionally, the aircraft will experience accelerations and decelerations during the flight course, in addition to the centripetal force shown above. For a level turn, the lift is directly proportional to the bank roll angle. During the flight course, operational precautions must be taken into account to reduce this force to avoid any structural failure.

3.1.2. Aerofoil Selection

The requirements of the project such as sustained flight, slow speed long duration flying could be met from the effects of high lift aerofoil aerodynamics. A high coefficient of lift is known to be achieved by an under cambered aerofoil [21]. The team researched and analysed a variety of aerofoils such as **E423, N10, NACA 4412, S1223** and **S7055** [22] using the flow simulation analysis on **XFLR5**.

The graphs of C_l Vs α, C_d Vs α, C_l Vs C_d from our analysis are given below:

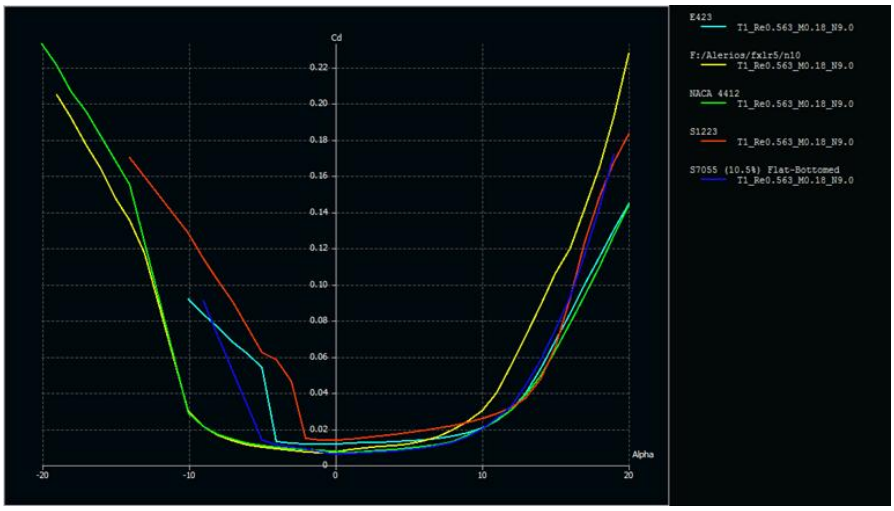

Fig. 3.2: Coefficient of drag, C_d Vs α

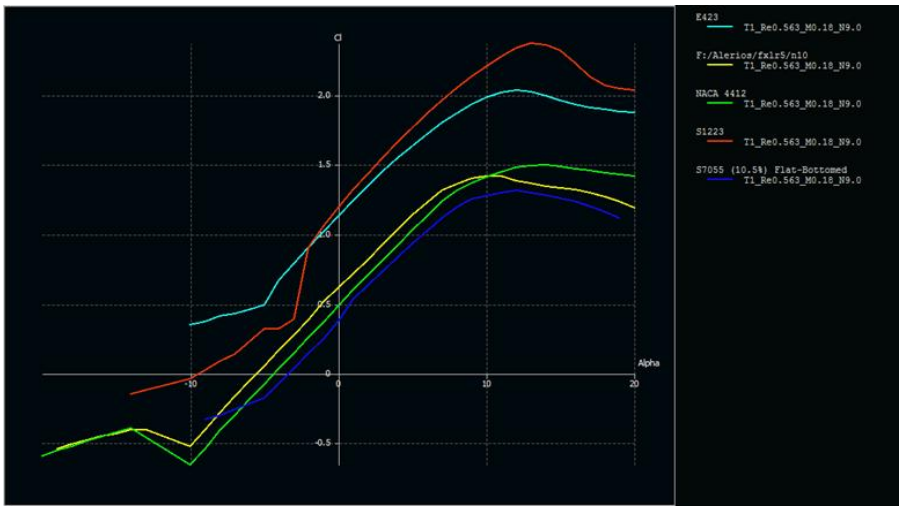

Fig. 3.3: Coefficient of lift, C_l Vs α

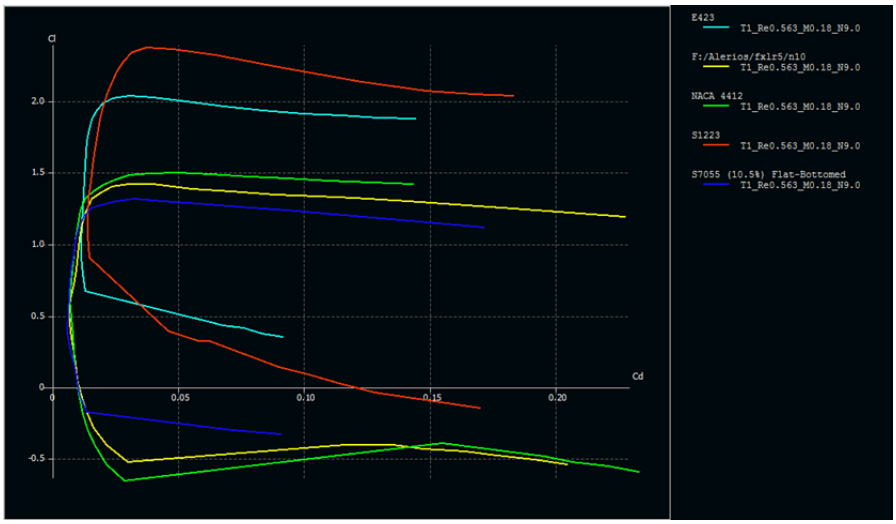

Fig. 3.4: Coefficient of lift, C_l Vs Coefficient of drag, C_d

As seen from the data, S1223 showed remarkable behaviour in comparison to the others.

The effect of camber was considered and due to the benefits, moderately to heavily camber aerofoils are usually used on RC aircrafts [21]. S1223 and E423 were the only aerofoils amongst those analysed which had the most preferable camber.

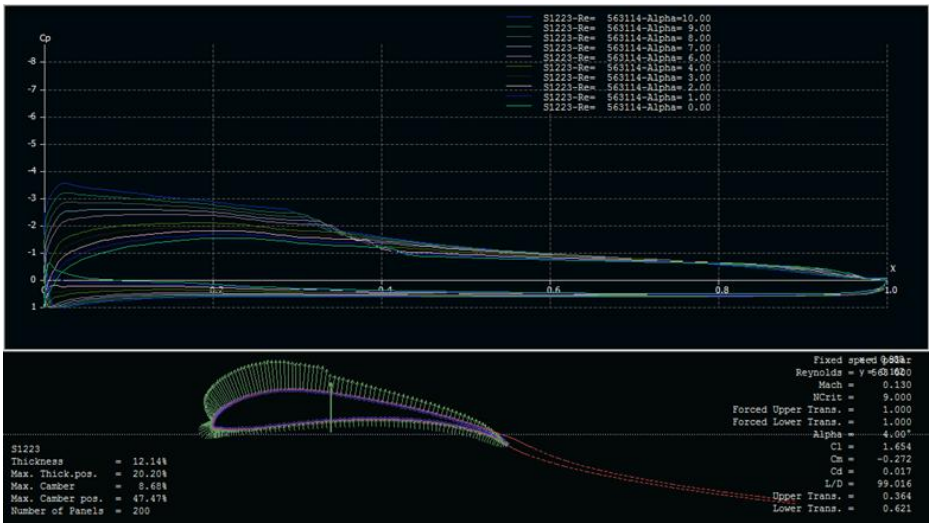

Fig. 3.5: Angle Variations on S1223

We decided to use an angle of attack of 3º as it would give optimum lift to drag value, while also reducing stall. Further research on the aerofoil S1223 [6], showed us that it had a high stalling angle of attack, high lifting coefficient even at low speeds, and less profile drag, all advantages which were in alignment with the constraints stated above. Even if the aerofoil came with certain cons like more induced drag, and high pitch down moment, these disadvantages would be compensated by positioning the wing directly on the centre of gravity (C.G.), and using elevators to counter the pitching moment.

3.1.3. Wing Planform

We considered different planforms and weighed out their advantages and disadvantages.

Table 3.1: Comparative Study of Different Plan Forms

	Advantages	Disadvantages
Tapered Rectangular	• Reduces Induced Drag • Better Lift Distribution than Straight Rectangular	• Stalls Outboard • Reduces Aileron Effectiveness • More likelihood of Spin • Needs Additional Material to Sustain Bending Moment
Straight Rectangular	• Ease of Fabrication • Economical	• Vortex Losses
Elliptical	• Reduced Vortex Losses • Better Aerodynamic Efficiency	• Complex to Fabricate • Tendency to Stall

3.1.4. Aspect Ratio

Aspect ratio is a measure of the wing span compared to its chord. For RC aircrafts, it is generally taken in between 5 to 8. A higher ratio is disadvantageous as it causes more bending moment at the end of the wing and lowers its manoeuvrability due to an increased moment of inertia. We also didn't require increased internal volume, a benefit of a low A.R. Therefore, an aspect ratio of 6 was chosen.

3.1.5. Wing Area

The wing area was calculated based on the net weight of the aircraft including payload and the resulting wing loading. The net weight of the aircraft was estimated to be 3-5kg including payload, and wing loading for a trainer RC plane empirically is to be up to 20 kg/m^2.

We calculated potential wing areas using the formula,

Wing Area = Weight/Wing Loading.

The results are tabulated here.

Table 3.2: Wing Areas for Different Wing Loadings

Weight (kg)	Wing Loading (kg/m^2)	Wing Area (m^2)	Wing Area (in^2)
5	20	0.25	387.56
5	19	0.26	403
	18	0.27	418.5
5	17	0.29	449.5
5	16	0.31	480
5	15	0.33	511
5	14	0.35	542.5
5	13	0.38	589

Table 3.3: Wing Loading Examples

Aircraft	Type	Introduction	MTOW	Wing area	kg/m²	lb/sqft
Monarch Butterfly	Animal	Cenozoic			0.168	0.034
birds[a]	Animal	Cretaceous			1–20	0.20–4.10[3]
bird flight upper critical limit					25	5.1[4]
Ozone Buzz Z3 MS	Paraglider	2010	75–95 kg (165–209 lb)	25.8 m^2 (278 sq ft)	2.9–3.7	0.59–0.76[5]
Wills Wing Sport 2 155	Hang glider	2004	94.8–139.8 kg (209–308 lb)	14.4 m^2 (155 sq ft)	6.6–9.7	1.4–2.0[6]
upper limit	Microlift glider	2008	220 kg (490 lb) max.	12.2 m^2 (131 sq ft) min.[b]	18	3.7[7]
UK CAA	microlight wing loading limit		450 kg (990 lb) max. [c]	18 m^2 (190 sq ft) min.[c]	25	5.1[8]
Schleicher ASW 22	sailplane	1981	1,023 kg (2,255 lb)	16.7 m^2 (180 sq ft)	61.3	12.6
Piper Warrior	General aviation	1960	1,055 kg (2,326 lb)	15.14 m^2 (163.0 sq ft)	69.7	14.3
Beech Baron	General aviation twin	1960	2,313 kg (5,099 lb)	18.5 m^2 (199 sq ft)	125	26
Supermarine Spitfire	WWII Fighter	1938	3,039 kg (6,700 lb)	22.48 m^2 (242.0 sq ft)	135	28
Beechcraft Airliner	Regional airliner	1968	4,727 kg (10,421 lb)	25.99 m^2 (279.8 sq ft)	182	37
Learjet 31	Business jet	1990	7,031 kg (15,501 lb)	24.57 m^2 (264.5 sq ft)	286	59
MiG-23	Variable-geometry fighter	1970	17,800 kg (39,200 lb)	34.16–37.35 m^2 (367.7–402.0 sq ft)	477–521	98–107
General Dynamics F-16	Multirole fighter	1978	19,200 kg (42,300 lb)	27.87 m^2 (300.0 sq ft)	688.9	141.1
Fokker F27	turboprop airliner	1958	19,773 kg (43,592 lb)	70 m^2 (750 sq ft)	282	58
McDonnell Douglas F-15	Air superiority fighter	1976	30,845 kg (68,002 lb)	56.5 m^2 (608 sq ft)	546	112
Fokker F28	Regional Jet	1969	33,000 kg (73,000 lb)	78.97 m^2 (850.0 sq ft)	418	86
Boeing 737-300	Narrow-body airliner	1984	62,820 kg (138,490 lb)	91.04 m^2 (979.9 sq ft)	690	140
Boeing 737-900	Narrow-body airliner	2001	84,139 kg (185,495 lb)	124.6 m^2 (1,341 sq ft)	675	138
Boeing 767	Wide-body airliner	1982	142,882 kg (315,001 lb)	283.3 m^2 (3,049 sq ft)	504	103
Concorde	Supersonic transport	1976	187,000 kg (412,000 lb)	358.2 m^2 (3,856 sq ft)	522	107
Boeing 777	Wide-body airliner	1995	247,200 kg (545,000 lb)	427.8 m^2 (4,605 sq ft)	578	118
Boeing 747	Large aircraft	1977	333,000 kg (734,000 lb)	511 m^2 (5,500 sq ft)	652	134
Airbus A380	Large aircraft	2007	575,000 kg (1,268,000 lb)	845 m^2 (9,100 sq ft)	680	140

We decided on an area of 0.5574 m^2, which gave a wing loading of 8.97 kg/m^2. This was well within the specified range of up to 20 kg/m^2. The chord length was already a constant parameter, decided at 0.3048 m. After considering the lifting capacities and

manufacturing ability of various span lengths, we decided to design a wing of span 1.8288 m. These dimensions were later verified using analytical software applications.

3.1.6. Dihedral

10 degrees rise after 0.6096 m from centre. The central 0.6096 m on each side is to be kept flat for maximum efficient lift. Dihedral provided to stabilize rolling moment during sideslip.

3.1.7. Horizontal and Vertical Stabilizer

The areas of stabilizers were determined from typical empirical relations [2]. The stabilizers were designed with a sweepback because it reduces drag, adds an aesthetic value, helps avoid problems with the CG and allows the spars to be conveniently placed [4].

Table 3.4: Stabilizer Details

	Typical Relations	**Calculations**
Horizontal Stabilizer	Aspect Ratio = 3 to 5 Taper Ratio = 0.3 to 0.6 Area = 0.2 × Wing Area Chord = 0.33 × Wing Chord	Needed Area = 0.2 × 0.5574m^2 = **0.1115m^2** Optimized Area = **0.0929m^2** , by visual inspection and to reduce taper ratio
Vertical Stabilizer	Aspect Ratio = 1 to 2 Taper Ratio = 0.3 to 0.6 Area = 0.1 × Wing Area Chord = 0.33 × Wing Chord Tip Chord = Taper Ratio × Wing Chord	Area = 0.1 × 0.5574 m = **0.0557 m^2** Optimized Area = **0.0529 m^2** Height = **0.254 m** One Vertical Stabilizer = 0.2134m × 0.254m = **0.0542 m^2**, A.R. = **1.19** is satisfied. Tip Chord= 0.47 × 0.2134 m = **0.1016 m** Reduced optimized area after sweep = 0.0542 m^2 - 0.0142 m^2 = **0.04 m^2** Total area with control surfaces = 0.04 m^2 + 0.129 m^2 = **0.0529 m^2**
Elevator, Rudder	0.3 × Stabilizer Area OR by Visual Insp.	Elevator Area=0.508m×0.06m = **0.03048 m^2** Rudder Area=0.254m×0.06m = **0.01524 m^2**

3.1.8. Fuselage

The fuselage is usually 70-75% of wing length, so we took the length as 1.3716 m. The aft portion of the fuselage is to be made of carbon fibre rod (length 0.635 m). The frontal portion was selected to be made from balsa wood and the strength to the structure is given by ply wood.

Carbon Fibre rod: (see reference 27)

Length, L = 25 in = 635 mm

Inner diameter, d = 18 mm

Outer diameter, D = 20 mm

Distance from Neutral Axis, y = 10 mm

Density = 1.6 g/cc

Ultimate Tensile Strength, S_{ut} = 0.35 GPa

$I = (\pi/64) (D^4-d^4)$

$I = 2700.98\ mm^4$ ----- eq. 1

Flexural Formula: $S_{ut} / y = M / I = E / R$ ----- eq. 2 (see reference 18)

$M = W \times L = 635W$ N-mm ----- eq. 3

From 1, 2 and 3,

W= 148.873 N = 15.176 kg (load carrying capacity for carbon fibre rod) ----- eq. a

Mass = Density × Volume = $(\pi/4) (D^2-d^2) L \times$ Density = 0.06 Kg ----- eq. b

Aluminium rod (same dimensions): (see reference 27)

Density = 2.7 g/cc

S_{yt} = 276 MPa

$I = (\pi/64) (D^4-d^4)$

$I = 2700.98\ mm^4$ ----- eq. 4

Flexural Formula: $S_{yt} / y = M / I = E / R$ ----- eq. 5 (see reference 18)

$M = W \times L = 635W$ N-mm ----- eq. 6

From 4, 5 and 6,

W = 117.397 N = 11.967 kg (load carrying capacity for aluminium rod) ----- eq. c

Mass = Density × Volume = $(\pi/4) (D^2-d^2) L \times$ Density = 0.102 kg ----- eq. d

From equations a, b, c and d, we can say that the Carbon Fibre rod has higher load carrying capacity and lower mass than Aluminium rod of same dimensions.

Therefore, we are using a Carbon Fibre rod for boom.

3.2. Analysis and Testing

Throughout the design process, different software applications like XFLR-5 and SimFlow were used to simulate our ideas. This helped us make decisions based on the information we extracted from the CAD. The analysis for our design coupled with the physical tests we conducted ensured that the design of our aircraft was air worthy.

3.2.1. FEM Analysis of Wing Structure

The CFD results were directly analogous to the wind tunnel testing done on SimFlow. The wing structure experiences various types of loads during its time of flight which incorporates take-off, ascension, voyage, arriving and landing. The stresses acting on the wing were then analysed, wing geometries were created and then meshed. The sizing option used was proximity and curvature. In body sizing, edge sizing and face mapping was then carried out.

3.2.2. CFD Analysis of 2D Aerofoil

Figure shows the CFD analysis done at a free stream velocity of 22.22 m/s, a Reynolds no. of 150000 for Selig 1223 aerofoil (calculated on airfoil tools/calculator/Reynolds number).

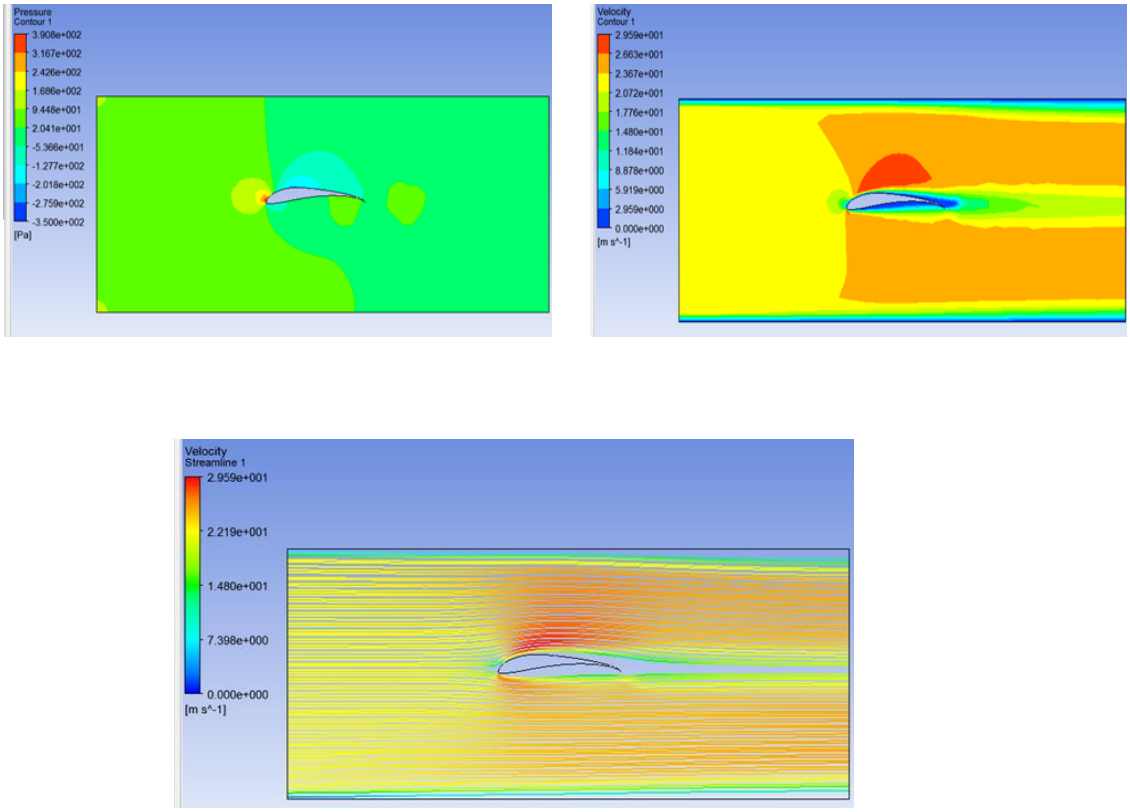

Fig. 3.6: CFD Analysis of 2D Aerofoil

3.1.7. 3D Wing Simulations

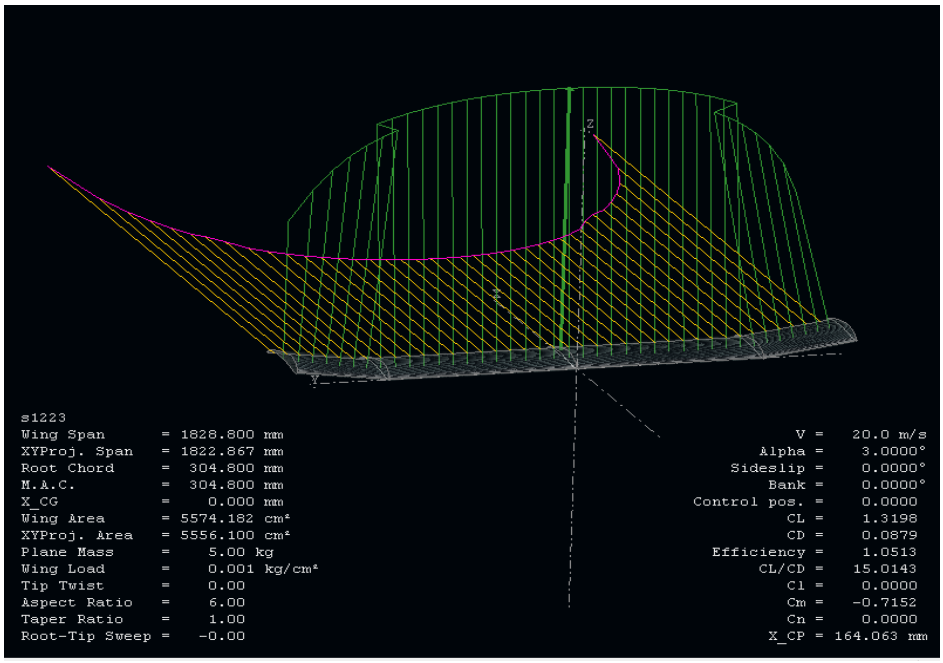

Fig. 3.7: Wing with Tip Dihedral 8˚

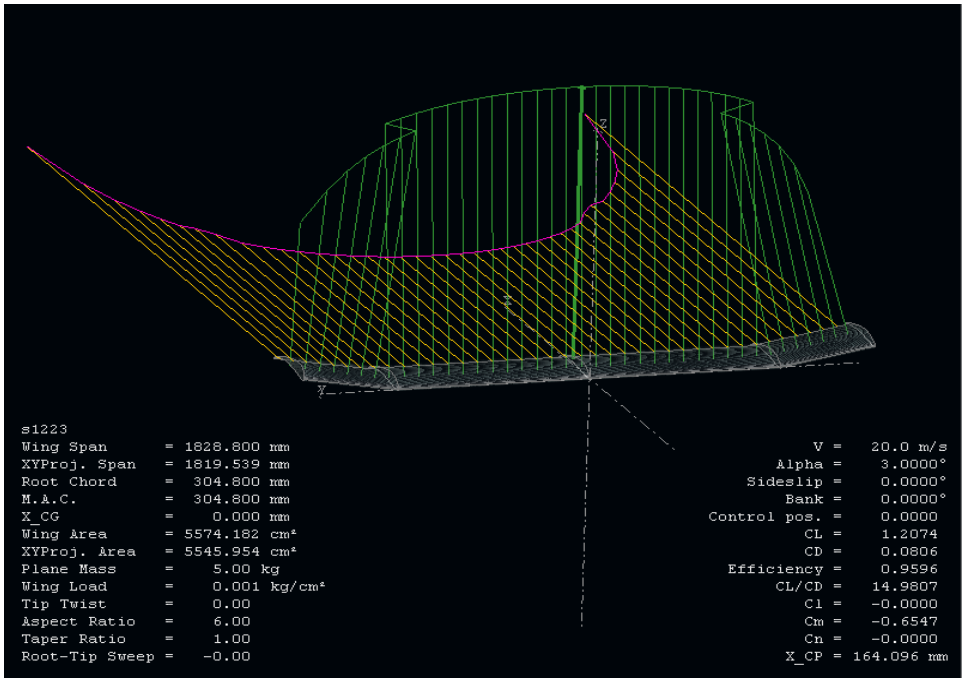

Fig. 3.8: Wing with Tip Dihedral 10˚

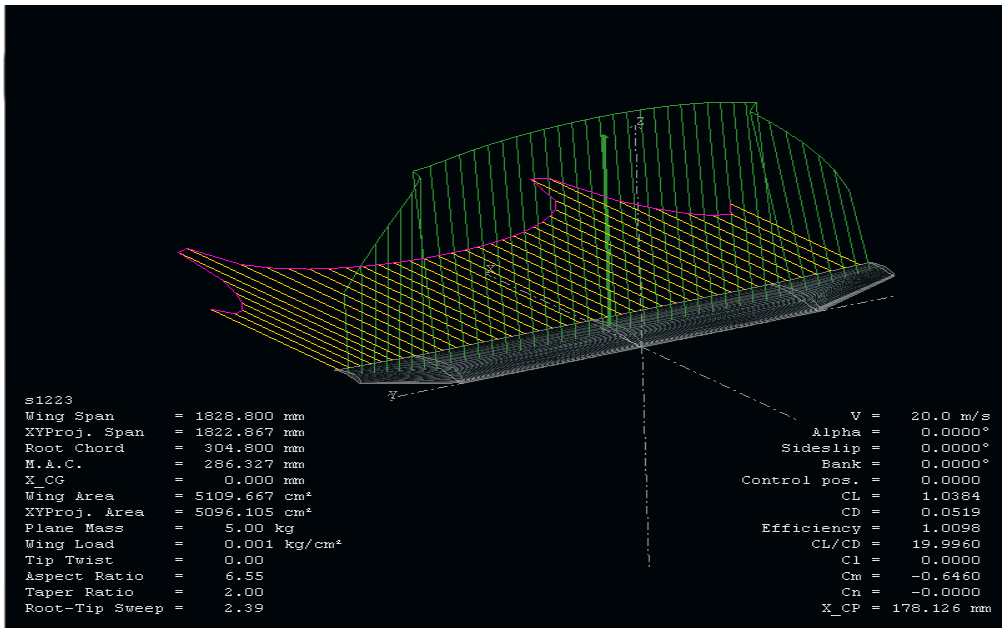

Fig. 3.9: Wing with Tapered Tips

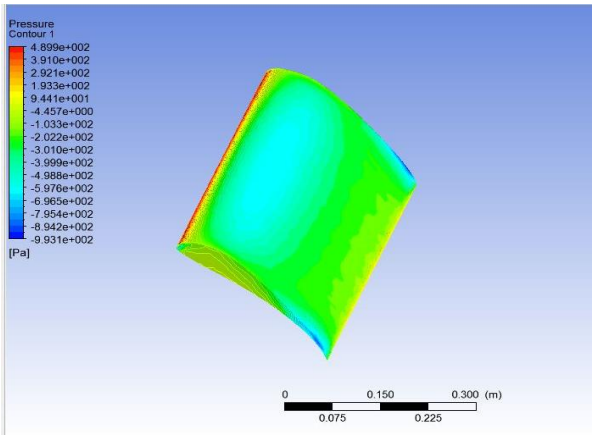

Fig. 3.10: Aileron at 0˚

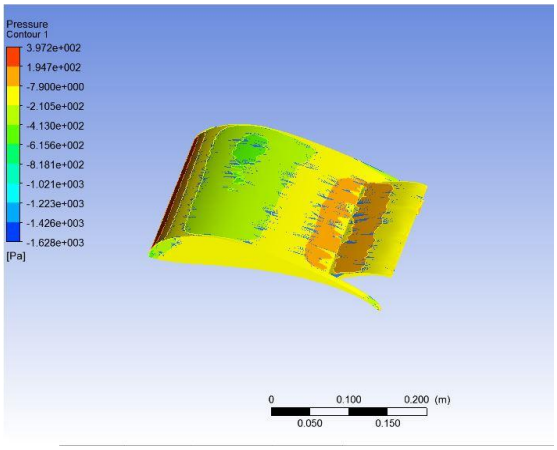

Fig. 3.11: Aileron at 30˚

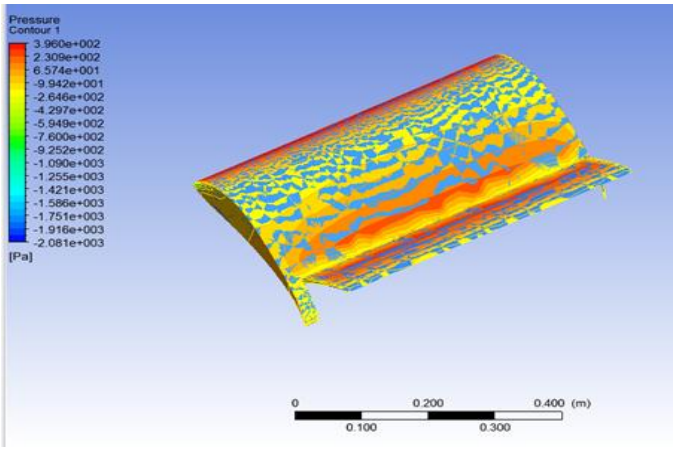

Fig. 3.12: Aileron at 60˚

3.3. Propulsion

The propulsion system was so designed to provide the necessary thrust to overcome the drag experienced during the flight. We selected O.S. Motor OMA 3815-1000 and a 3000mAh Lithium Polymer battery which would provide the required thrust for the following constant parameters.

• KV = RPM / Voltage = 1000

• Maximum Voltage = 11.1 V

• Maximum RPM = 11100 rpm

• Prescribed Propeller = 11” × 7” = 0.2794 m × 0.1778 m

3.4. Electronics and Other Components

Table 3.5: Electronics and Other Components

Component	Specifications	Additional Information
Motor	O.S. Motor OMA 3815-1000 RPM/Voltage: 1000kV Max. Constant Current: 50A No Load Current: 2.5A Constant Watts: 1800 Burst Watts: 740 Weight: 125g	Verification of thrust producing capability is provided in the propulsion section.
Battery and Charger	Lithium Polymer Capacity: 3000 mAh Voltage: 11.1 V Max. Continuous Discharge: 30C Weight: 200 g Dimensions: 137×45×18 mm Charger Voltage: 12.6 V	Flight time: Time (min) = mAh×10^{-3} /current drawn = 3000×10^{-3}×60/50 (burst) = 3.6 minutes 3000/1000×30C = 90 A This is safe current draw.
Servomotors	Futaba Servomotor S3003 Operating Voltage: 4.8-6 V 4.8 V: • 0.23 sec/60 degree rotation • 3.2 kg.cm Stall torque 6.0 V: • 0.19 sec/60 degree rotation • 4.1 kg.cm Stall torque	- Excessive torque is unnecessary as no strategic manoeuvres in air are needed - Comes with plastic ball bearing for smoother operation - Torque produced is high enough to overcome the wind force.
ESC	80 Amp Li-Po 3S With BEC	- Higher rating decreases chances of failure by overheating
Transmitter	Futaba 6EX 2.4 GHz radio set	

Propeller	0.2794m × 0.254m Electric	- Slow fly propellers are used for low speed applications, and have more efficiency - Consider the 0.254m×0.127m to 0.2794m×0.254m range - 0.2794m×0.254m propeller was tested and verified during motor test
Solar Panels	Sunpower C60 125mm × 125mm Efficiency: 22% Vpp: 0.57V Ipp: 5.8A Peak Power: 3.3 W	
Charge Controller	3S 12V 10A 18650 Lithium Battery Charger Board Protection Module	-Ensures security of battery pack by avoiding overcharging. -Increases battery life.

3.5. Photovoltaic Energy Conversion

3.5.1. Solar Power Management System

Energy received from the Sun is collected by the solar panel, which converts it into electricity and then there is the maximum power point tracker (MPPT), which helps in tracking the maximum power of any solar cell and provides it at all times. [9]

In level flight, the MPPT sends power directly to the motor from the solar cells and, when gliding, as the motor does not require power, the battery starts charging. [9]

If an excess of power is required, during climbing or when the solar intensity is low, the battery supplies the required power. [9]

From the battery, the energy goes to the motor, which rotates the propeller and, between them, there is an electronic speed control (ESC) regulating the speed. [9]

The solar power management system incorporates a DC-DC converter and MPPT algorithm inside a Battery Management System (BMS) microcontroller. The microcontroller is used to sense the input and output power to perform MPPT operation and to generate gate pulse for DC-DC converter. The purpose of BMS is to monitor each cell and to avoid over-charging of battery, hence increasing the battery life. The first step in the design of solar power system is to identify the power demand and the maximum power that can be generated with the available surface area. [8]

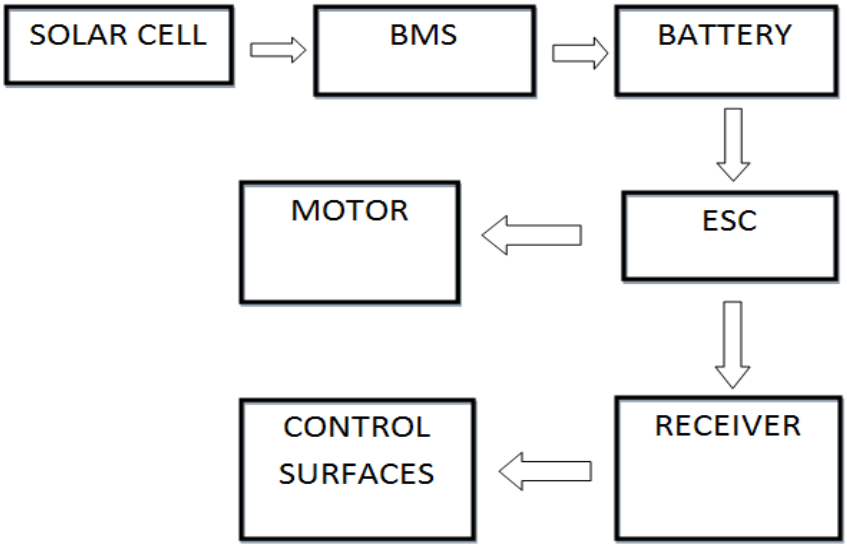

Fig. 3.13: Solar Power Management System

3.5.2. Battery Management System (BMS)

The battery management system monitors and controls the storage and delivery of the energy drawn from the solar panels. Lithium–ion Polymer (Li-Po) batteries are less tolerant to overcharging. Battery Management System (BMS) is used to avoid overcharging of the individual cells. Commercially available Li-Po batteries have individual cells connected in series to provide the required voltage, 3-cell and 4-cell batteries are commonly used, as shown in figure. [8]

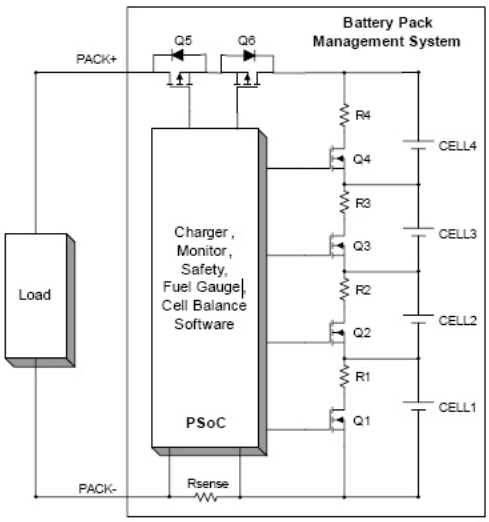

Fig. 3.14: Battery Management System [2]

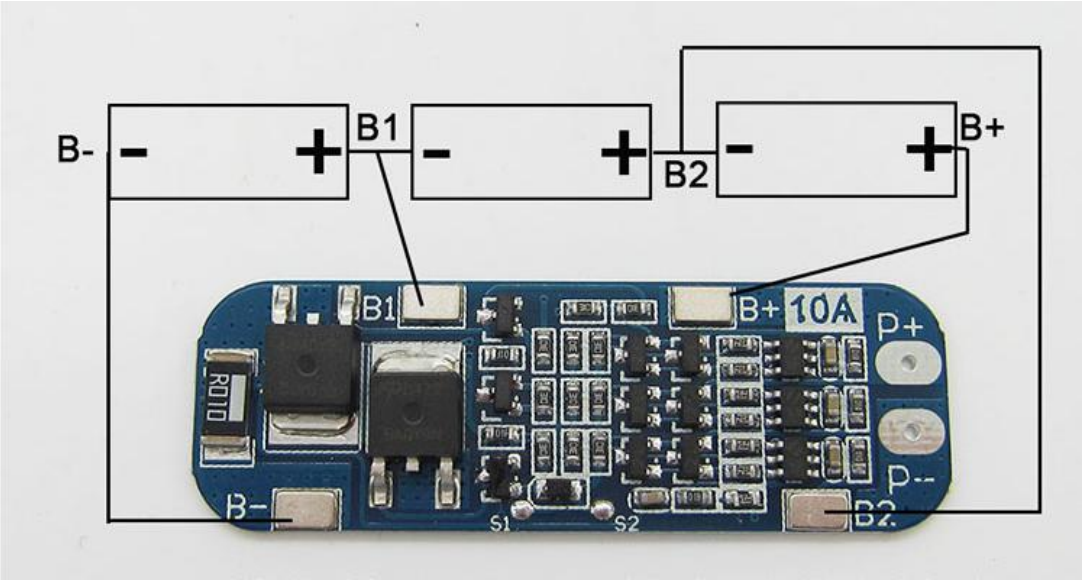

Fig. 3.15: Charge Controller

Specifications (3S 10A 12V 18650 Lithium Battery Charger Board Protection Module) -

1. Size: 53 x 17 x 4 mm.
2. Over discharge voltage range : 2.3-3.0 v ± 0.05
3. Recharge voltage range: 4.25-4.35 v ± 0.05 v
4. Operating current : 6-8A
5. Operating temperature : -40 to + 50 ℃
6. Current limit : 10-13A

7. Storage condition : -40- + 80 ℃
8. Resting current : less than 30uA
9. Effective lifetime : over 30,000 hours
10. Internal resistance : less than 100mΩ
11. Short-circuit protection.
12. Self-recovery delay.
13. Charging Voltage: 12.6 V-13 V.
14. Over-charge, over-discharge, over-current, short circuit protection.

3.5.3. Maximum Power Point Tracking (MPPT)

The electric power generated from the solar cells depends on the temperature and the solar radiation conditions and the load electric characteristics. MPPT is often used in photovoltaic systems to maximize the solar panel output power, irrespective of the temperature and irradiation conditions and of the load electrical characteristics. It is performed by the microcontroller. [8]

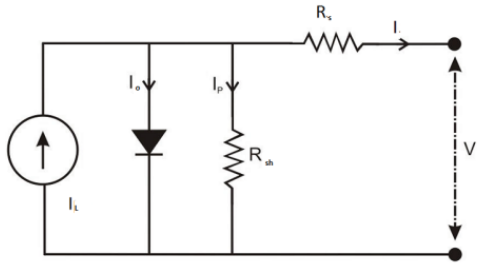

Fig. 3.16: Solar Cell represented as a Non Linear Current Source [8]

The solar cell is a nonlinear device and can be represented as a current source model as shown in Figure 9, where I is the equivalent current source, R_{sh} and R are the shunt and series resistance of the material and D is the P-N junction diode.

In order to efficiently use the solar cells, we attempt to force the solar cells to operate at the maximum power point through some mechanism called the MPPT. At maximum power point $\Delta P/\Delta V = 0$. We decrease the output voltage if $\Delta P/\Delta V < 0$, and increase output voltage while $\Delta P/\Delta V > 0$. [9]

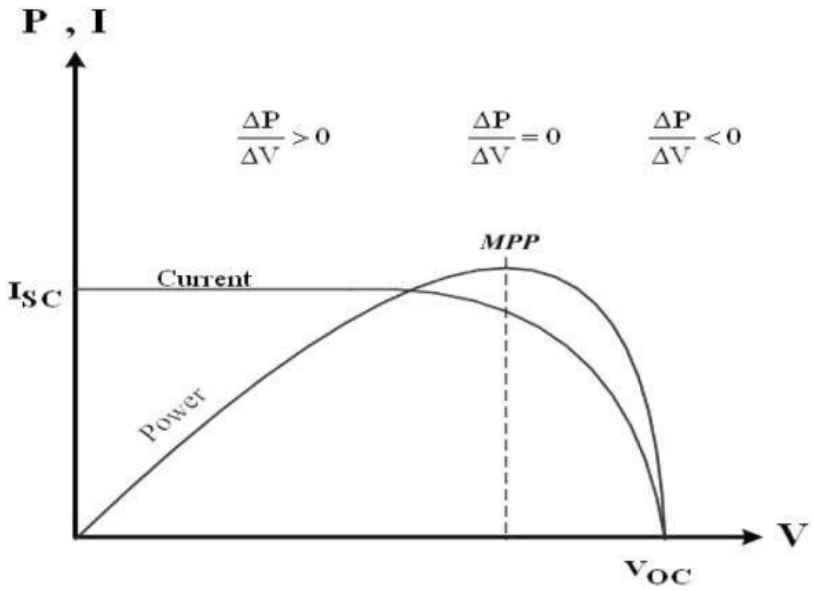

Fig. 3.17: Solar Panel Characteristics [8]

3.5.4 Battery Selection

Energy storage is necessary in case of decrease in solar irradiance due to clouds and also to increase the reliability of the system. Rechargeable batteries are the most preferred choice of energy storage medium. Commercially available batteries and their specifications are given in table.

Lithium - ion polymer battery is preferred as it has high efficiency, power and considerably high energy density (Table 6).

In this application, 3S LiPo arrangement is used to avoid a very large wingspan (for > 3S) and low power output (for < 3S). [8]

Table 3.6: Battery Selection [8]

Battery	Energy Density (Wh/Kg)	Power (W/Kg)	Efficiency (%)
Lead-acid	30-40	180	70-92
Nickel Cadmium	40-60	150	70-90
Lithium- ion	150-250	1800	99
Lithium-ion Polymer	130-200	3000+	99.8

Battery Specifications - LiPo 3S, 30C rating, 3000mAh, 11.1 V. [8]

The battery requires 12.6 V for charging.

The primary load connected to the solar cell is the electric motor (used to propel the aircraft). The battery and load is connected directly to the output of DC/DC converter. The battery gets charged when the power available from the PV module is higher than the power required by the load and vice-versa for discharging.

3.5.5 Cell Selection

Sunpower C60 monocrystalline Silicon Photovoltaic cells are selected as they have higher efficiency (22%) than typical silicon based solar cells (about 15%). [9]

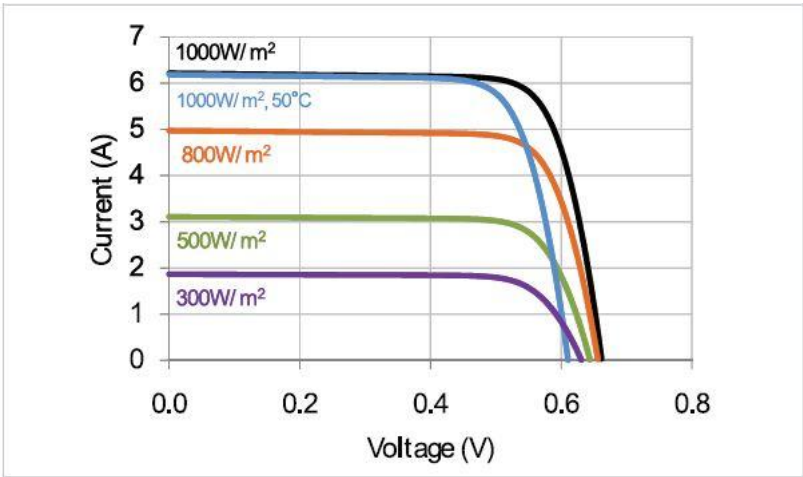

Fig. 3.18: Sunpower C60 I-V characteristics

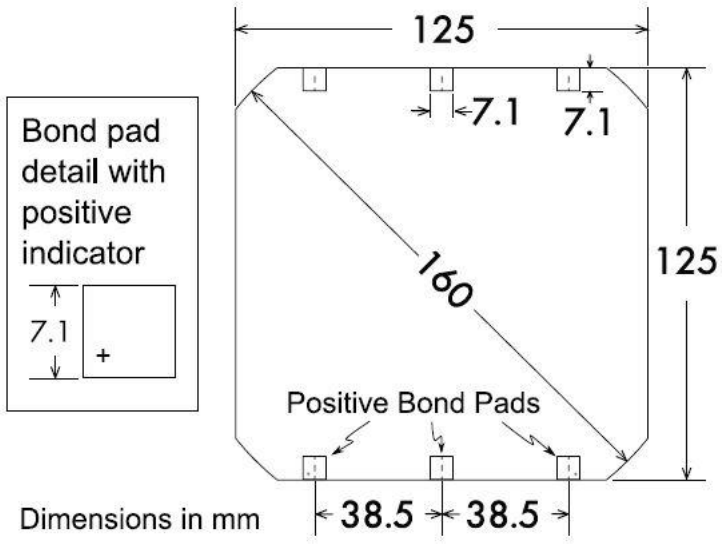

Bond pad area dimensions are 7.1mm x 7.1mm
Positive pole bond pad side has "+" indicator on leftmost and rightmost bond pads.

Fig. 3.19: Cell Dimensions

Table 3.7: Sunpower C60 Physical Characteristics

Physical Characteristics	
Construction:	All back contact
Dimensions:	125mm x 125mm (nominal)
Thickness:	165µm ± 40µm
Diameter:	160mm (nominal)

Table 3.8: Sunpower C60 Electrical Characteristics

Electrical Characteristics of Typical Cell at Standard Test Conditions (STC) STC: 1000W/m², AM 1.5g and cell temp 25°C						
Bin	Pmpp (Wp)	Eff. (%)	Vmpp (V)	Impp (A)	Voc (V)	Isc (A)
G	3.34	21.8	0.574	5.83	0.682	6.24
H	3.38	22.1	0.577	5.87	0.684	6.26
I	3.40	22.3	0.581	5.90	0.686	6.27
J	3.42	22.5	0.582	5.93	0.687	6.28
All Electrical Characteristics parameters are nominal Unlaminated Cell Temperature Coefficients Voltage: -1.8 mV / °C Power: -0.32% / °C						

These readings were recorded at Standard Test Conditions i.e. solar irradiation of one kilowatt (kW) per square metre, a module temperature of 25 degrees Celsius and a solar irradiation angle of 45 degrees. [9]

Table 3.9: Sunpower C60 Cell Specifications [9]

Mass of Solar cell	0.008 Kg
Length and Width	0.125 m 0.125 m
Area of single solar panel	0.0150 m^2
Efficiency of solar cell	22%
Rated Voltage	0.57 V
Rated Current	5.37 A

From above table, peak power generated by each cell = V × I = 3.34W. [9]

Number of solar cells required is given by -

N = (Voltage required to charge the battery) / (Voltage produced by each cell)

i.e. N = 12.6/0.57 = 22.1

Therefore, 22 Sunpower C60 cells are required.

Also, 2 additional panels are added for safety. So, 24 panels are required.

Mass of each cell is 0.008 kg; therefore mass of 24 cells is 0.192 kg.

This is the load produced by the solar cells on the wings.

Power generated by each cell is 3.34 W.

So, peak power generated by the panel (24 cells) is 80.16 W.

3.5.6 Solar Cells Arrangement

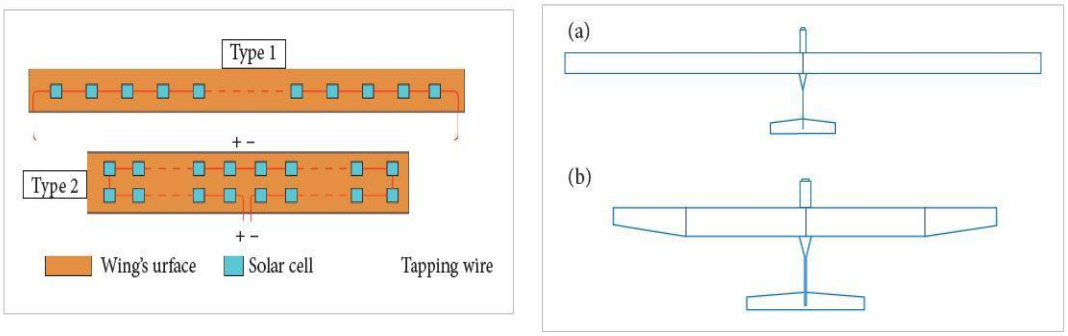

Fig. 3.20: Solar Cells Arrangement [9]

As can be seen from above figures, in 1st case wingspan required will be more which increases weight and cost. Also longer wiring will be required which will reduce efficiency. In 2nd case, the design is more compact as well as provided with ailerons which increases stability. Hence this arrangement is preferred.

Hence, 12 cells in 2 rows can be arranged, giving the minimum area covered by the cells as 1500 mm × 250 mm as per the dimensions of each cell.

3.6. Weight Balance

Table 3.10: Weight Balance

COMPONENT	WEIGHT (Kg)	MOMENT ARM (cm)	MOMENT (Kg-cm)
M	0.194	42 (fore)	8.148
E1	0.289	32 (fore)	9.248
A (C.G.)	0.208	0 (at C.G.)	0
E2	0.096	29 (aft)	2.784
E3 + S	1.600	9.1325 (aft)	14.612

Centre of gravity at 0.36 m from firewall (front).

M: Motor + Propeller

E1: ESC + BMS + Battery + Receiver

A: Air Quality Analyser

E2: Servos

E3 + S: Servos in wing + Total Structural

Sum of moments: 8.148 + 9.248 + 0 – 2.784 – 14.612 = 17.396 – 17.396 = 0

Hence, C.G. is balanced.

The total weight of model is 0.194 + 0.289 + 0.208 + 0.096 + 1.600 = 2.387 Kg.

3.7. Air Quality Analyser

We have finalised AtmoTube Plus, of all those shortlisted air quality analysers from the market.

AtmoTube is a portable device that monitors the quality and safety of the air you breathe. It measures real-time air pollution caused by harmful gases and a wide range of Volatile Organic Compounds (VOCs) like acetone, methanol, benzene, ethanol, toluene, xylene, and formaldehyde. It also measures atmosphere pressure, temperature, and humidity. It constantly monitors the air around you and immediately alerts you when the air is not safe.

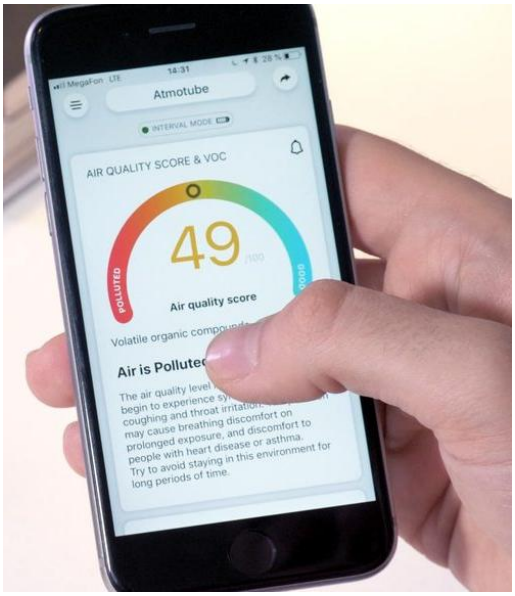

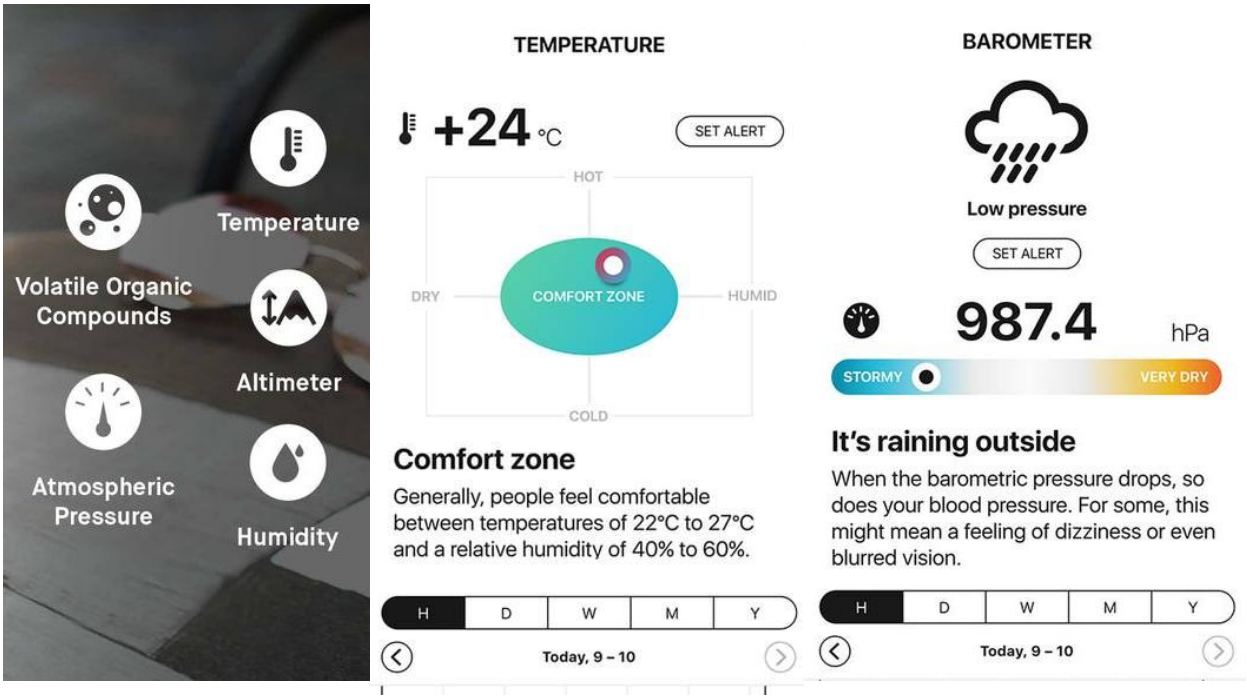

Fig. 3.21: AtmoTube, App User Interface

Features:

- Accurate and reliable air quality sensing as MEMS TVOC sensor does not require any human calibrations.
- Barometric pressure sensor provides more useful information and real-time alerts to weather changes.
- Monitors air temperature and humidity.
- Latest technology (USB-C type for charging which lasts for 7 days on single charge, improved antenna performance helps connection to smart phone upto 30 feet via Bluetooth 5.0).
- Dimensions: Height: 66 mm, Width: 22 mm, Weight: 38

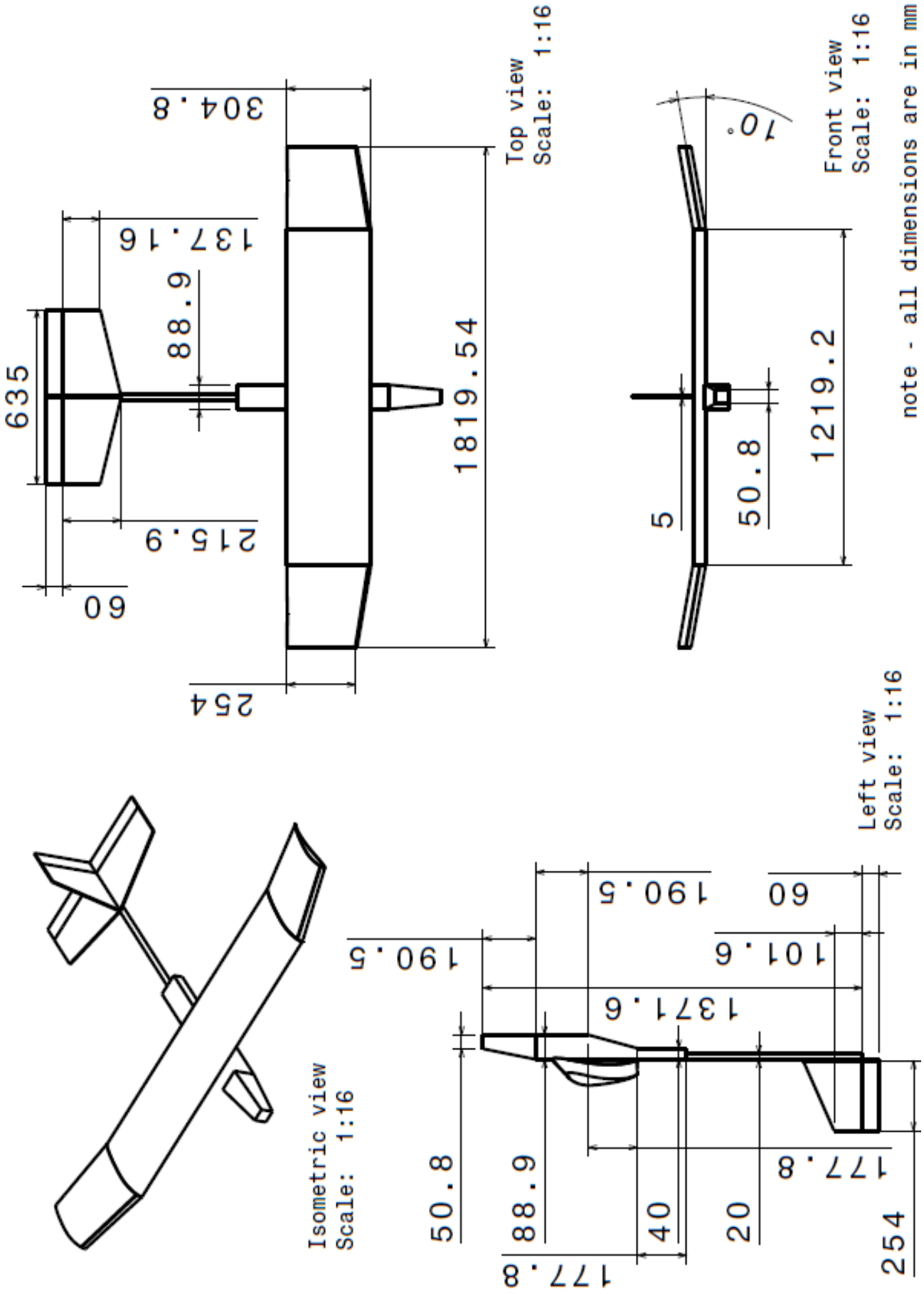

Fig. 3.22: Drafting

3.8. Manufacturing

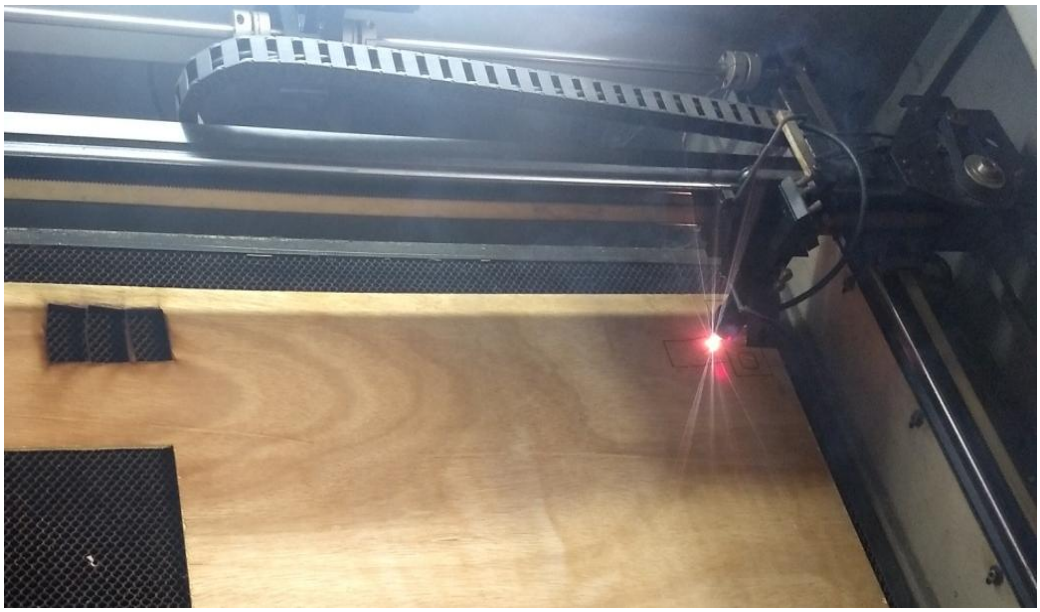

Fig. 3.23: Laser Cutting

Fig. 3.24: Wing (ribs)

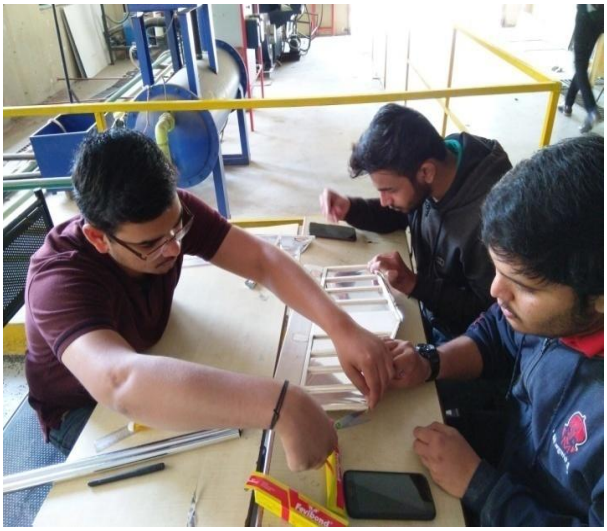

Fig. 3.25: Tail

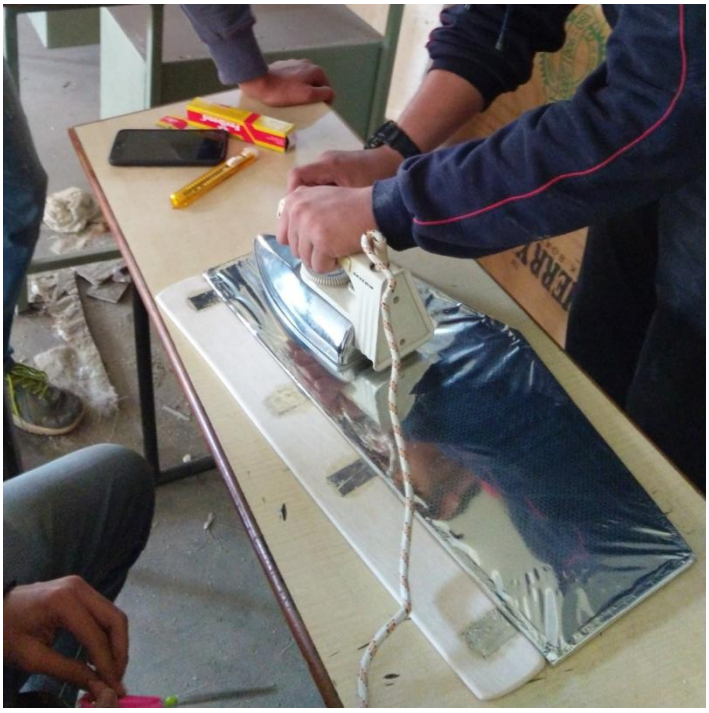

Fig. 3.26: Heat Ironing

Fig. 3.27: Fuselage

Fig. 3.28: Soldering of solar cells

CHAPTER FOUR

EXPERIMENTAL VALIDATION

4. EXPERIMENTAL VALIDATION

Flight Test Photos: 1st Flight

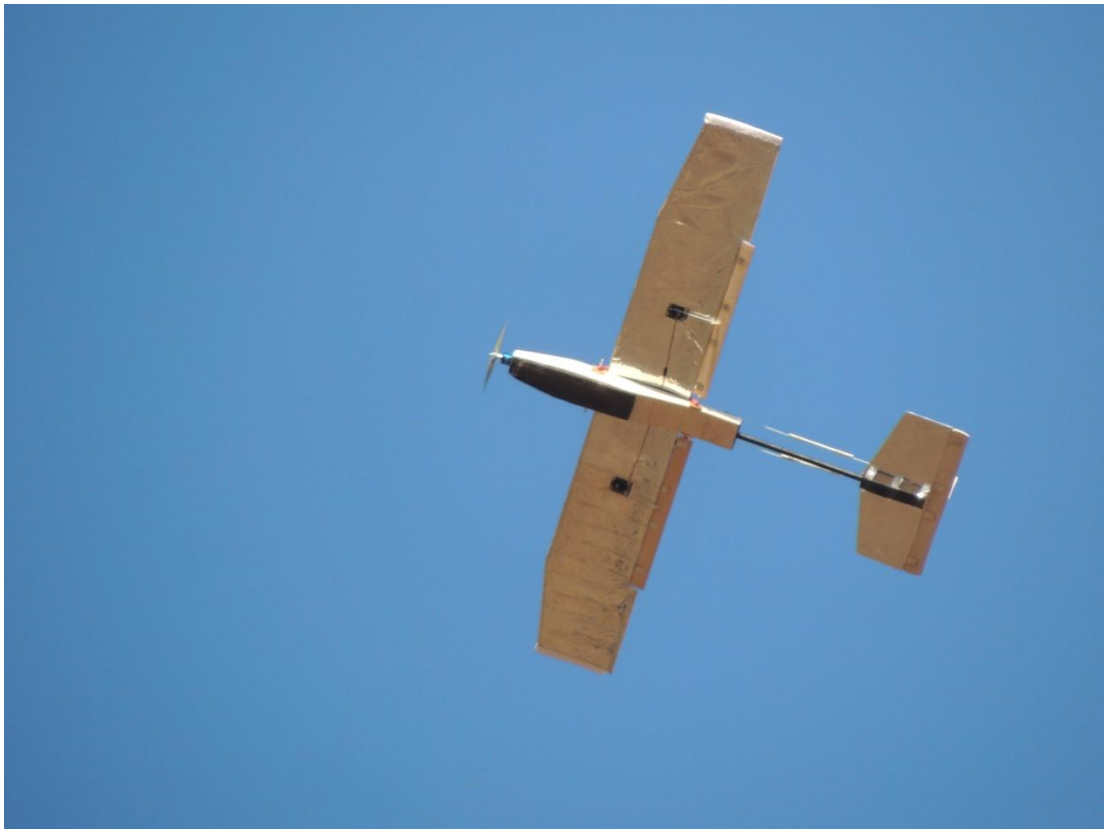

2nd Flight (After Modifications)

Fig. 4.1: Flight

4.1. Modifications after Flight Tests

Table 4.1: Design Modifications

	Modifications	Calculations
Horizontal Stabilizer	Stabilizer area increased to increase pitching stability	Designed Area = **0. 1115m^2** Current Area = Chord × Length = 0.1524 m × 0.508 m = **0.0929 m^2** Needed Area = 0.25 to 0.28 x 0.5574 m^2 Modified Area = 0.267 × 0.5574 = **0.1492 m^2**
Wing	Taper given to wing tip for reducing drag and increasing stability	Designed area = 0.5574 m^2 Modified area = 0.5419 m^2

4.2. Solar Charging Characteristics (at different hours over a period of 3 days)

Date: 06/04/2019

Table 4.2: Solar Charging on 6th April

a) Time: 10.30 AM (Table 4.2.1)

Time Duration (min.)	Voltage (Volts)
0	11.7
5	11.9
10	12.0
15	12.1
20	12.2

b) Time: 1.15 PM (Table 4.2.2)

Time Duration (min.)	Voltage (Volts)
0	11.2
5	11.5
10	11.7
15	11.8
20	11.9

c) Time: 4.30 PM (Table 4.2.3)

Time Duration (min.)	Voltage (Volts)
0	11.0
5	11.4
10	11.6
15	11.7
20	11.9

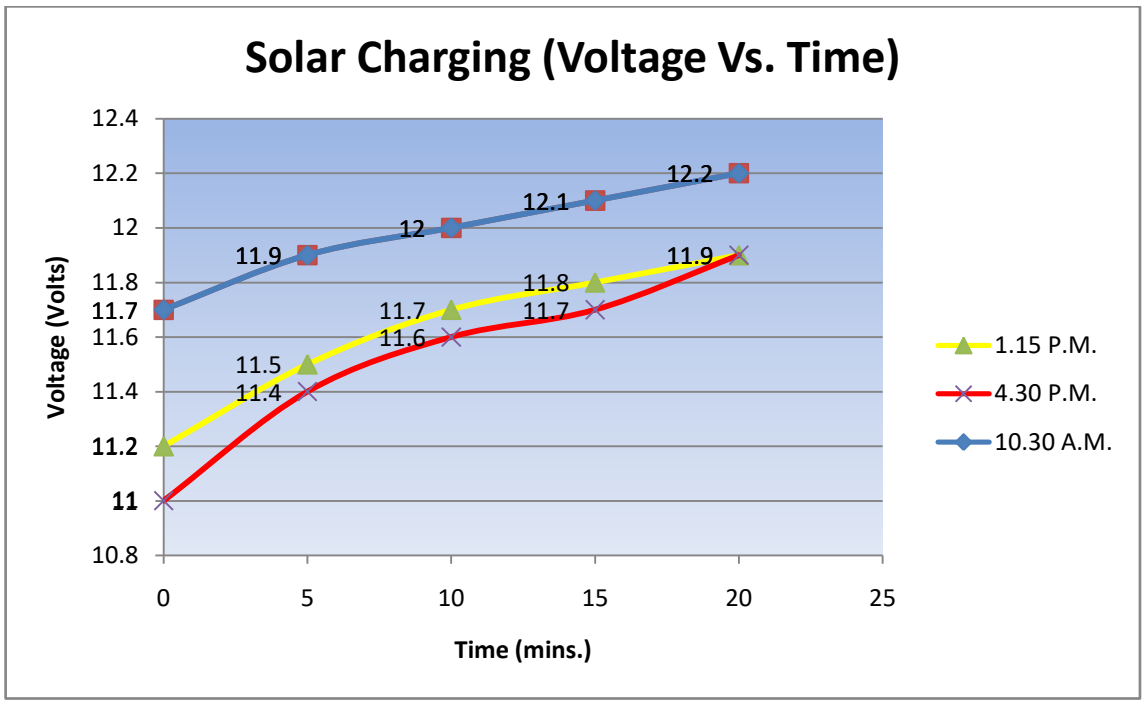

Fig. 4.2: Solar Charging Characteristics Graph

Date: 07/04/2019

Table 4.3: Solar Charging on 7th April

a) Time: 10.15 AM (Table 4.3.1)

Time Duration (min.)	Voltage (Volts)
0	11.0
5	11.4
10	11.6
15	11.8
20	11.9

b) Time: 1.15 PM (Table 4.3.2)

Time Duration (min.)	Voltage (Volts)
0	10.6
5	11.3
10	11.6
15	11.7
20	11.9

c) Time: 4.05 PM (Table 4.3.3)

Time Duration (min.)	Voltage (Volts)
0	10.1
5	11.1
10	11.3
15	11.5
20	11.6

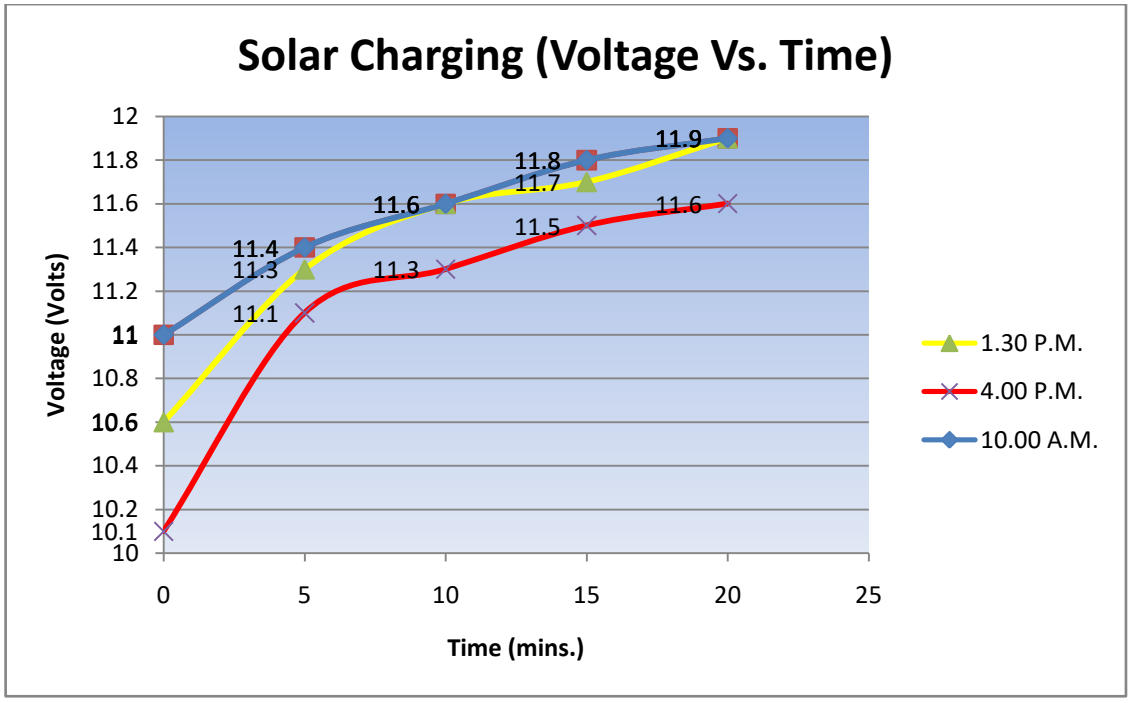

Fig. 4.3: Solar Charging Characteristics Graph

Date: 08/04/2019

Table 4.4: Solar Charging on 8th April

a) Time: 10.00 AM (Table 4.4.1)

Time Duration (min.)	Voltage (Volts)
0	10.8
5	11.3
10	11.5
15	11.6
20	11.8

b) Time: 1.30 PM (Table 4.4.2)

Time Duration (min.)	Voltage (Volts)
0	9.9
5	11.2
10	11.5
15	11.6
20	11.7

c) Time: 4.00 PM (Table 4.4.3)

Time Duration (min.)	Voltage (Volts)
0	10.3
5	11.2
10	11.4
15	11.6
20	11.7

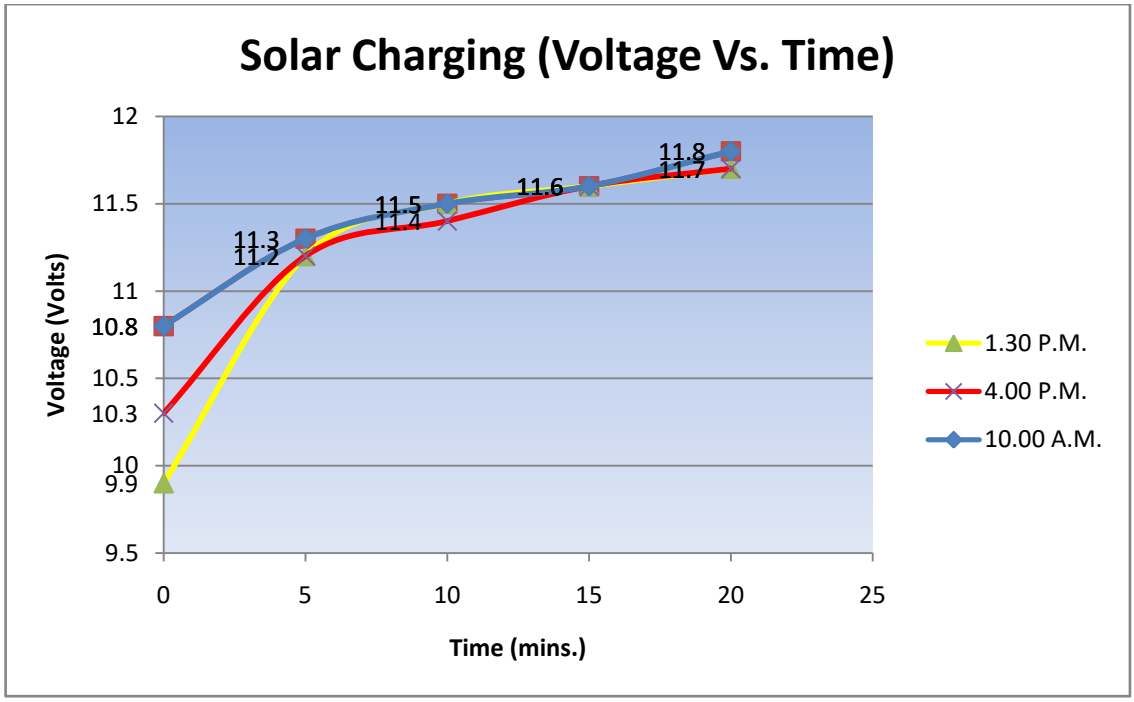

Fig. 4.4: Solar Charging Characteristics Graph

4.3. Battery Discharge Characteristics

a) Without solar power, at constant throttle.

Table 4.5: Battery Discharge Characteristics (Without Solar Power)

Initial Voltage (Volts)	Final Voltage (Volts)	Time Duration (min.)
12.1	11.8	5
11.6	11.2	5
11.2	9.95	5

b) With solar power, at constant throttle.

Table 4.6: Battery Discharge Characteristics (With Solar Power)

Initial Voltage (Volts)	Final Voltage (Volts)	Time Duration (min.)
12.1	12.0	5
11.6	11.5	5
11.2	11.1	5

Calculations:

a) Range 1, initial voltage at 0 min. = 12.1 V

Discharge percentage:

Without solar = ((12.1 – 11.8)/12.1) = (0.3/12.1) × 100 = 2.48%

With solar = ((12.1 – 12)/12.1) = (0.1/12.1) × 100 = 0.83%

Therefore, percentage reduction in discharge rate is

((2.48 - 0.83)/2.48) = (1.65/2.48) × 100 = 66.53%

b) Range 2, initial voltage at 0 min. = 11.6 V

Discharge percentage:

Without solar = ((11.6 – 11.2)/11.6) = (0.4/11.6) × 100 = 3.45%

With solar = ((11.6 – 11.5)/11.6) = (0.1/11.6) × 100 = 0.86%

Therefore, percentage reduction in discharge rate is

((3.45 - 0.86)/3.45) = (2.59/3.45) × 100 = 75.07%

c) Range 3, initial voltage at 0 min. = 11.2 V

Discharge percentage:

Without solar = ((11.2 – 9.95)/11.2) = (1.25/11.2) × 100 = 11.16%

With solar = ((11.2 – 11.1)/11.2) = (0.1/11.2) × 100 = 0.89%

Therefore, percentage reduction in discharge rate is

((11.16 - 0.89)/11.16) = (10.27/11.16) × 100 = 92.03%

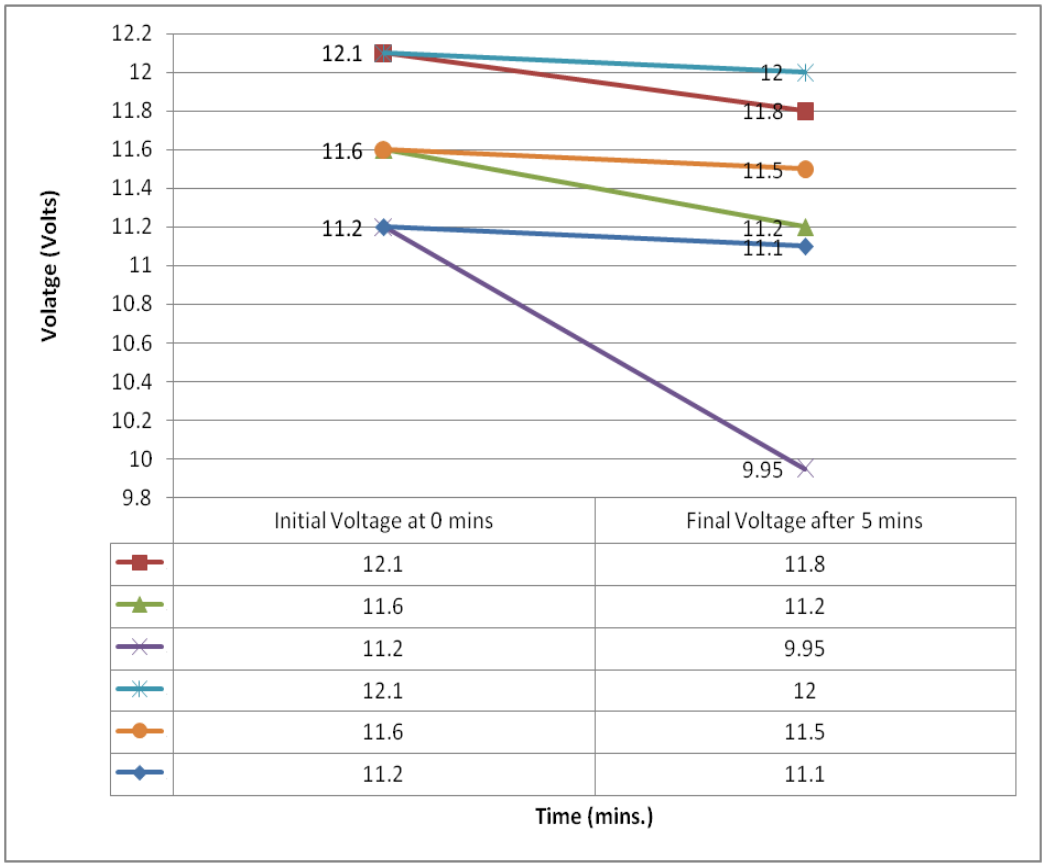

Fig. 4.5: Solar Discharging Characteristics Graph

4.4. **Solar Array Output** at different configurations

Date: 09/04/2019

Time: 2.15 PM

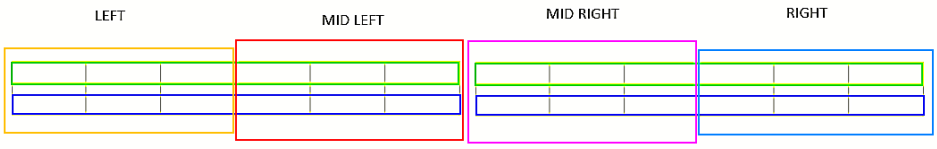

Fig. 4.6: Solar Cell Array Nomenclatures

Table 4.7: Solar Array Output for different configurations

a) 25% cells exposed

Configuration	**Voltage (Volts)**	**Current (Ampere)**
Left 6 open	8.91	0.03
Mid left 6 open	7.95	0.03
Mid right 6 open	6.45	0.03
Right 6 open	6.58	0.03

b) 50% cells exposed

Configuration	**Voltage (Volts)**	**Current (Ampere)**
Left wing open	8.49	0.03
Right wing open	7.74	0.04
Upper array open	9.8	0.04
Lower array open	11.4	0.06

c) 75% cells exposed

Configuration	**Voltage (Volts)**	**Current (Ampere)**
Left 6 covered	10.0	0.06
Mid left 6 covered	10.96	0.04
Mid right 6 covered	11.46	0.05
Right 6 covered	11.59	0.05

d) 100% cells exposed

Configuration	**Voltage (Volts)**	**Current (Ampere)**
All open	**13.58**	**3.72**

4.5. Efficiency

Theoretical power per cell as per manufacturer's catalogue is 3.34 Watts.

Thus, total theoretical power = 24 × 3.34 = 80.16 Watts

Actual power = Voltage × Current = 13.58 × 3.72 = 50.5176 Watts

Efficiency of the system is [(Actual power / Theoretical power) × 100]

= (50.5176 / 80.16) × 100 = **63.0209%**

4.6. Thrust vs. Throttle

Table 4.8: Thrust-Throttle values for different Propellers

Propeller	At 25% Throttle	At 50%	At 70%	At 100%
10x7E	0.15 kg Thrust	0.35 kg	0.75 kg	1.2 kg
11x7SF	0.2 kg	0.5 kg	1.0 kg	1.5 kg
11x10E	0.2 kg	0.5 kg	1.1 kg	1.6 kg

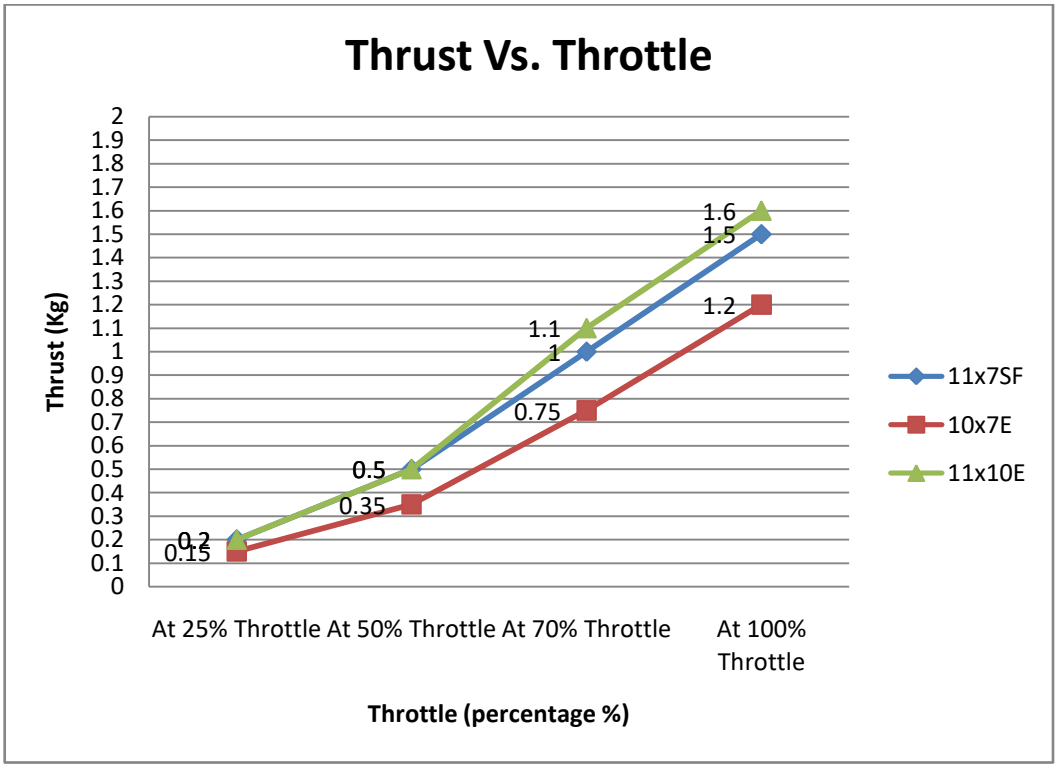

Fig. 4.7: Motor Thrust Vs. Throttle Graph

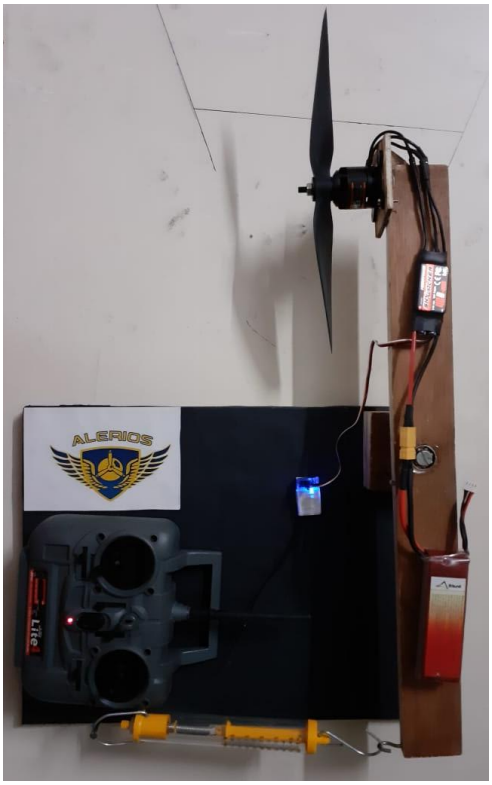

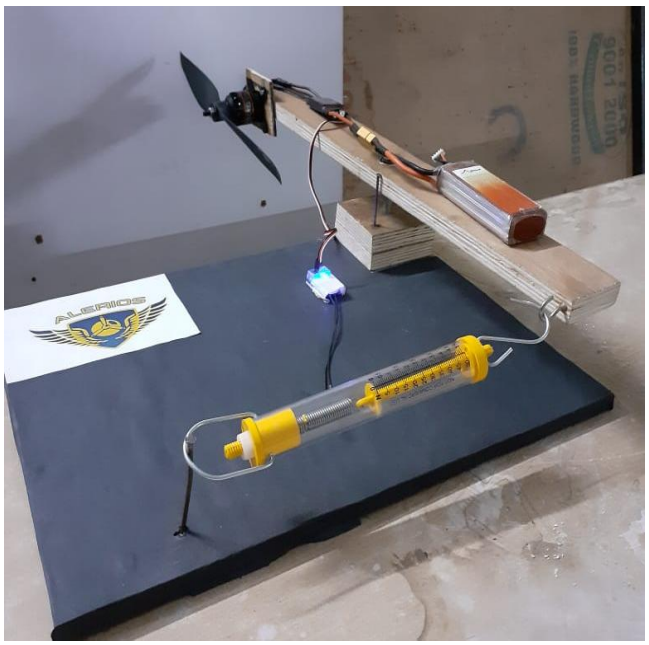

Fig. 4.8: Thrust Rig

4.7. Air Quality Data Sheet

Table 4.9: AtmoTube Data Sheet

Date Time	VOCs (ppm)	Air Quality Score	Temperature (°C)	Humidity (%)	Pressure (mbar)	Latitude	Longitude
22-03-2019 8:30	0	100	28.3	25	927.1	18.4436	73.84177
22-03-2019 8:31	0	100	29.2	22	927	18.4436	73.84177
22-03-2019 8:32	0	100	30.1	24	927.1	18.4436	73.84177
22-03-2019 8:33	0	100	31.3	20	927.2	18.4436	73.84177
22-03-2019 8:34	0	100	31.6	18	927	18.43519	73.84246
22-03-2019 8:35	0	100	26.3	18	922	18.43519	73.84246
22-03-2019 8:36	0	100	26.6	18	922.8	18.43519	73.84246
22-03-2019 8:37	0	100	26.2	18	918.5	18.43519	73.84246
22-03-2019 8:38	0	100	26.6	18	927	18.43944	73.84217
22-03-2019 8:39	0	100	27.1	18	927.2	18.43944	73.84217
22-03-2019 8:40	0	100	29.1	17	927.1	18.4436	73.84177
22-03-2019 8:41	0	100	30.1	18	927.1	18.4436	73.84177
22-03-2019 8:42	0	100	30.4	18	927.1	18.4436	73.84177
22-03-2019 8:43	0	100	31	19	927.2	18.4436	73.84177
22-03-2019 8:44	0	100	31.9	22	927.2	18.4436	73.84177

22-03-2019 8:45	0	100	32.7	32	927.2	18.43519	73.84246
22-03-2019 8:46	0.007	99	33.3	33	927.3	18.43519	73.84246
22-03-2019 8:47	0.028	98	33.7	34	927.3	18.43616	73.84141
22-03-2019 8:48	0.029	98	34	31	927.2	18.43616	73.84141
22-03-2019 8:49	0.053	96	34.1	29	927.3	18.43988	73.84159
22-03-2019 8:50	0.036	97	34	28	927.3	18.43988	73.84159
22-03-2019 8:51	0.022	98	33.9	26	927.3	18.45658	73.8443
22-03-2019 8:52	0.046	97	34.1	28	927.3	18.45434	73.85165
22-03-2019 8:53	0.058	96	34.4	29	927.2	18.4436	73.84177
22-03-2019 8:54	0.05	97	34.8	29	927	18.4436	73.84177
22-03-2019 8:55	0.05	97	34.9	29	927.1	18.4436	73.84177
22-03-2019 8:56	0.033	98	35.1	28	927.1	18.4436	73.84177
22-03-2019 8:57	0	100	35	28	927.09	-	-
22-03-2019 8:58	0	100	35	26	927.06	-	-
22-03-2019 9:00	0.031	98	35.2	29	927.1	18.4436	73.84177
22-03-2019 9:01	0.01	99	34.9	28	932.5	18.4436	73.84177
22-03-2019 9:02	0	100	34.9	27	936.7	18.4436	73.84177
22-03-2019 9:03	0.002	99	34.8	28	937.9	18.45359	73.85119
22-03-2019 9:04	0.004	99	34.8	28	939	18.43616	73.84141
22-03-2019 9:05	0.055	96	34.8	29	939.6	18.42725	73.83781
22-03-2019 9:06	0	100	34.6	26	939.5	18.4277	73.83857
22-03-2019 9:07	0.019	98	34.4	26	939.6	18.42758	73.83842
22-03-2019 9:08	0.034	97	34.2	25	939.7	18.42756	73.83836
22-03-2019 9:09	0.044	97	33.9	25	939.6	18.4277	73.83857
22-03-2019 9:10	0.051	96	33.8	25	939.7	18.4276	73.83851
22-03-2019 9:11	0.056	96	33.7	25	939.7	18.4276	73.83854

4.8. Design Failure Modes Effect and Analysis (DFMEA)

Table 4.10: Design Failure Modes Effect and Analysis

Component or Process	Potential Failure Mode	Effect	Causes	S	O	D	RPN	Recommended Action
Fuselage	Structural failure, Breaking of Fuselage	Overall damage to Fuse	Failure of structural members due to excessive load	8	4	9	288	Choose appropriate adhesive and high factor of safety (FOS) materials, effective design and analysis; constant testing

Landing Gear	Impact Loading	Damage to Fuselage and Propeller	Inappropriate material and improper contact of the landing gear with the fuselage	10	5	4	200	Use of Spring Steel for heavy aircrafts and foam for lighter aircrafts to sustain impact loading conditions.
Motor	Over-Heating	Loss of Motor	Closed enclosure with minimal air circulation for heat exchange	9	7	2	126	Placing the motor open to atmosphere for easy heat circulation
Wing	Wind Shear Loading	Loss of stability and ultimate result in aircraft failure	Nut bolt fixture completely constraint the movement due to wind shear	7	5	6	210	Using rubber bands instead of nut bolts which would distribute the loading rather than concentrating it. The bolting will result in cracking.
Tail	Structural Failure	Failure of Tail Assembly	Improper assembly leads to separation of tail from fuselage.	8	4	4	128	Using proper and strong tail mounts and good assembly techniques to avoid tail failure

CHAPTER FIVE

CONCLUSION

AND

FUTURE SCOPE

5. CONCLUSION AND FUTURE SCOPE

5.1. Conclusion

The design of the airframe along with the energy calculations and selection of components were done after studying the reference material. CAD model of the airframe has been designed using CATIA V5 and simulations have been performed using XFLR5. Materials were selected by considering its weight and strength. The electrical and electronic components were selected according to their specifications which best matched our requirements. The Air Quality Analyser – AtmoTube was shortlisted based on its weight and functionality, corresponding to our requirement.

The structural integrity has been validated using various simulations and flight tests. The experimental validation was completed in two stages, viz. On-ground testing and In-flight testing. Certain modifications in airframe were made in compliance with the observations from both In-flight and On-ground tests.

The solar cells were tested in various conditions of inbound radiations, of both beam and diffused types. The solar cells were tested for charging of LiPo Battery over a period of 3 days at different time intervals, at different voltages, and relevant graphs were plotted in accordance to these variables to understand the charging characteristics better. Solar cell outputs for different solar cell array configurations were studied to understand the effect of shadow on the different parts of array on the wing. The total output of the array is 13.58 volts and 3.72 amperes. The efficiency of the solar system was found out to be 63.021%

The battery discharge characteristics were studied for the system with and without solar energy input. The percent reduction in discharge rate of the battery was found out for different ranges. It was found that the reduction in discharge rate was higher when the battery is at lower initial voltage.

For range 1, percentage reduction in discharge rate was 66.53%.

For range 2, it was 75.07%.

And, for range 3, it was 92.03%.

Differences in Voltage (Initial – Final) for battery were studied, for both with and without the use of solar cells and it was found that the difference was greater when the solar cells were not connected to the battery. Thus it was observed that the percentage drop in discharge rate was greater at lower voltages, as the charging at lower voltages is faster, which was verified experimentally.

The selected Air Quality measurement device - AtmoTube, was successfully installed on the UAV model and operated in flight testing to obtain the results in the app, which were later converted into a datasheet for better understanding and analysis.

5.2. Future Scope

Autopilot system can be installed in the model, to eliminate the need of experienced human flyers. In autopilot mode, the vehicle is controlled by computer software instead of manual remote control. The position of the drone is updated at very small intervals, to the computer via GPS, and it travels on the selected present route, speed and altitude.

In our project, we have used solar powered glider to analyse air quality. Similarly, this model can be used for other applications like surveillance, tracking, inspection in areas which are difficult to access manually, rescue operations, etc.

Dual batteries can be installed with a switching circuit to increase the flight time. When one of the two batteries is used it discharges, at the very same time, second battery is charging from the solar cells. These two batteries are connected to the control board which is further connected to the load as well as the solar panels. The control board switches one battery from charging terminals to load terminals and other battery from load terminals to charging terminals automatically based on the amount of charge present in the battery or any other preset parameters. However, this arrangement requires use of complicated circuits, which then increases cost and also increases the weight. Hence, we used a single battery system in our project, to keep the weight as well as the cost as minimum as possible.

REFERENCES

1. Aditya A Paranjape, Soon-Jo Chung and Michael S Selig, 'Flight mechanics of a tailless articulated wing aircraft' (Published 12 April 2011, 2011 IOP Publishing Ltd), Bioinspiration & Biomimetics, Volume 6, Number 2
2. S. Jashnani, T.R. Nada , M. Ishfaq, A. Khamker, P. Shaholia, 'Sizing and preliminary hardware testing of solar powered UAV', Volume 16, Issue 2, December 2013, Pages 189-198
3. Stanley R. Herwitz, 'Solar-powered UAV Mission for Agricultural Decision Support', Conference: Geoscience and Remote Sensing Symposium, 2003. IGARSS '03. Proceedings. 2003 IEEE International, Volume: 3
4. Philipp Oettershagen1, Amir Melzer, Thomas Mantel, Konrad Rudin, Rainer Lotz, Dieter Siebenmann, Stefan Leutenegger, Kostas Alexis and Roland Siegwart, 'A Solar-Powered Hand-Launchable UAV for Low-Altitude Multi-Day Continuous Flight', Journal of Field Robotics (JFR), 2015, pp 3986-3993,
5. Prof. E.G. Tulapurkara, 'Airplane design (Aerodynamic)' (Chpt 6, Lecture 23 to 30)
6. Selig, Michael S. and Guglielmo, James J. "High-Lift Low Reynolds Number Airfoil Design." Journal of Aircraft No. 1 Vol. 34. (1997)
7. Amertha A, Krishnakumar, 'Solar Based Drive System For Aerial Vehicles', ISSN: 2320 – 8791, 2013 pp. 1-5
8. Karthik Reddy Buchireddy Sri, Poondla Aneesh, Kiran Bhanu, M Natarajan, 'Design Analysis of Solar-Powered Unmanned Aerial Vehicle', J. Aerosp. Technol. Manag., São José dos Campos, Vol. 8, No. 4, pp. 397-407, Oct.-Dec., 2016
9. Mohd Rizwan Sirajuddin Shaikh, Santosh B. Waghmare, Suvarna Shankar Labade, Pooja Vittal Fuke, Anil Tekale, 'A Review Paper on Electricity Generation from Solar Energy', Volume 5 Issue IX, September 2017
10. S.P.Sukhatme, J.P Nayak 'Solar energy:principles of thermal collection and storage,third edition',Pp 313-315,McGraw Hill education (India) pvt. Ltd.
11. Parvathy Rajendran, Nurul Musfirah Mazlan and Howard Smith, 'Single Cell Li-Ion Polymer Battery Charge and Discharge Characterizations for

Application on Solar-Powered Unmanned Aerial Vehicle', Key Engineering Materials, Vol. 728, pp. 428-433, 2017

12. Yevgen Barsukov, Texas Instruments 'Battery Cell Balancing: What to Balance and How'

13. Prabir Patra, Shyam Lal, B H Subbayya (Physical Research Laboratory, Navrangpura, Ahmedabad, India), Charles H Jackman (NASA Goddard Space Flight Center, Greenbelt, Maryland), P. Rajaratnam (Indian Space Research Organization, Antriksh Bhavan, Bangalore, India), 'Observed vertical profile of sulfur hexafluoride and its atmospheric application', Journal of Geophysical Research, Vol. 2, no. D7, pp. 8855-8859, April 20, 2015

14. Philipp Oettershagen1, Amir Melzer, Thomas Mantel, Konrad Rudin, Rainer Lotz, Dieter iebenmann, Stefan Leutenegger, Kostas Alexis and Roland Siegwart in 'A Solar-Powered Hand-Launchable UAV for Low-Altitude Multi-Day Continuous Flight' published by the Journal of Field Robotics (JFR), 2015, pp

15. Sarath K. Guttikonda, Rahul Goel, Pallavi Pant , 'Nature of air pollution, emission sources and management in the Indian cities', Atmospheric Environment, Volume 95, October 2014, pp. 501-510

16. Bisht DS, Tiwari S, Dumka UC, Srivastava AK, Safai PD, Ghude SD, Chate DM, Rao PSP, Ali K, Prabhakaran T, Panickar AS, Soni VK, Attri SD, Tunved P, Chakrabarty RK, Hopke PK, 'Tethered balloon-born and ground-based measurements of black carbon and particulate profiles within the lower troposphere during the foggy period in Delhi, India', Science of The Total Environment, Vol. 573, 15 December 2016, pp. 894-905

17. Stephen W. Moore, Peter J. Schneider (Delphi Automotive Systems), 'A Review of Cell Equalization Methods for Lithium Ion and Lithium Polymer Battery Systems'.

18. Polly E. Langa, David C. Carslaw, Sarah J. Moller in 'A trend analysis approach for air quality network data'.

19. Peter Garrison, Rectangular Wings, Flying Magazine, January 1, 2003 (article)

20. Grant E. Carichner, Leland M. Nicolai, 'Fundamentals of Aircraft and Airship Design, Volume 2 - Airship Design and Case Studies' **BOOK**

21. RCadvisor's Model Airplane Design Made Easy, Carlos Reyes **BOOK**

22. S. Ramamrutham, R. Narayan, Strength of Materials **BOOK**

23. Senator John H. Glenn, Jr., in 'NASA's Let It Glide' **PDF**

24. Alejandro Diaz Puebla and Raghu Chaitanya Munjulury, in 'Sizing Of actuators for flight control systems and flaps integrations in Rapid' **PDF**

25. Ideen Sadrehaghighi, in 'Aerodynamic Design & Optimization' **PDF**

26. SAE Aero Design Workshop, Chennai

27. Airfoil Tools (http://airfoiltools.com/index)

28. Gerry Yarrish, Flying with Flaps - What You Need to Know, Model Airplane News (https://www.modelairplanenews.com/flap-facts-flying-and-setting-up-rc-planes-with-flaps/)

29. NASA, 'Induced Drag Coefficient' (https://www.grc.nasa.gov/www/k-12/airplane/induced.html)

30. Air pollution declines with height (https://www.scidev.net/asia-pacific/pollution/news/air-pollution-decline-with-height.html)

31. National Air Quality Index, Control of Urban Pollution Series (CPUS), June2018 (http://www.cpcb.nic.in)

32. http://www.performance-composites.com/carbonfibre/mechanicalproperties_2.asp